

EDGE DETECTION METHODS FOR SPECKLED IMAGES

CENTRE FOR NEWFOUNDLAND STUDIES

**TOTAL OF 10 PAGES ONLY
MAY BE XEROXED**

(Without Author's Permission)

GANUGAPATI SESHU SRILAKSHMI



INFORMATION TO USERS

This manuscript has been reproduced from the microfilm master. UMI films the text directly from the original or copy submitted. Thus, some thesis and dissertation copies are in typewriter face, while others may be from any type of computer printer.

The quality of this reproduction is dependent upon the quality of the copy submitted. Broken or indistinct print, colored or poor quality illustrations and photographs, print bleedthrough, substandard margins, and improper alignment can adversely affect reproduction.

In the unlikely event that the author did not send UMI a complete manuscript and there are missing pages, these will be noted. Also, if unauthorized copyright material had to be removed, a note will indicate the deletion.

Oversize materials (e.g., maps, drawings, charts) are reproduced by sectioning the original, beginning at the upper left-hand corner and continuing from left to right in equal sections with small overlaps. Each original is also photographed in one exposure and is included in reduced form at the back of the book.

Photographs included in the original manuscript have been reproduced xerographically in this copy. Higher quality 6" x 9" black and white photographic prints are available for any photographs or illustrations appearing in this copy for an additional charge. Contact UMI directly to order.

UMI

A Bell & Howell Information Company
300 North Zeeb Road, Ann Arbor MI 48106-1346 USA
313/761-4700 800/521-0600

EDGE DETECTION METHODS FOR SPECKLED IMAGES

by

© Ganugapati Seshu Srilakshmi, B.Tech.,

A thesis submitted to the School of Graduate
Studies in partial fulfillment of the
requirements for the degree of
Master of Engineering

Faculty of Engineering and Applied Science
Memorial University of Newfoundland
July, 1996

St. John's

Newfoundland

Canada



National Library
of Canada

Acquisitions and
Bibliographic Services

395 Wellington Street
Ottawa ON K1A 0N4
Canada

Bibliothèque nationale
du Canada

Acquisitions et
services bibliographiques

395, rue Wellington
Ottawa ON K1A 0N4
Canada

Your file Votre référence

Our file Notre référence

The author has granted a non-exclusive licence allowing the National Library of Canada to reproduce, loan, distribute or sell copies of this thesis in microform, paper or electronic formats.

The author retains ownership of the copyright in this thesis. Neither the thesis nor substantial extracts from it may be printed or otherwise reproduced without the author's permission.

L'auteur a accordé une licence non exclusive permettant à la Bibliothèque nationale du Canada de reproduire, prêter, distribuer ou vendre des copies de cette thèse sous la forme de microfiche/film, de reproduction sur papier ou sur format électronique.

L'auteur conserve la propriété du droit d'auteur qui protège cette thèse. Ni la thèse ni des extraits substantiels de celle-ci ne doivent être imprimés ou autrement reproduits sans son autorisation.

0-612-23137-2

Abstract

Images obtained from coherent imaging systems such as laser, sonar, radar, synthetic aperture radar (SAR) and ultrasound are often corrupted by a phenomenon known as image speckle. Speckle is characterized as multiplicatively signal dependent and may be spatially highly correlated noise. It differs from other types of noise such as the additive white Gaussian noise (AWGN) most commonly found in digital images. Observed from a human or computer vision point of view speckle gives a granular patterned appearance to images, thus obscuring underlying image details.

Gradient methods taking differences between pixel values may give inconsistent estimates regarding true edge pixels and therefore are not suited for use with speckled images. By contrast, taking ratios between the pixel values tends to factor out the multiplicative noise effect present in speckled images and to generate meaningful edge maps for these images. But these methods generate thick and ambiguous edge maps, and may also require gradient information supporting the ratio edge strength values in order to generate better edge maps on speckled images. This thesis investigates methods to improve the performance of existing speckle specific edge detection operators. A ratio edge detector based on maximum strength edge pruning (MSPRoA) which uses both edge strength magnitude and direction is proposed.

The MSPRoA method is different from previous methods in that it uses the edge orientation information that is implicitly expressed in some other ratio based methods, explicitly, thus enabling the generation of precise and well defined edge maps for speckled images. The MSPRoA method does not require either gradient information or edge thinning operators and hence computational savings are achieved. The use of the MSPRoA at multiple scales in order to extract edge information at both micro and

macro levels is also suggested. The MSPRoA and multi-scale MSPRoA methods are tested using both synthetic and real airborne SAR images of varying scene contents and business. Test results which confirm the suitability of the method for use on speckled images are presented. The use of the MSPRoA method is recommended for detecting edges images in which speckle phenomena are manifest.

Acknowledgements

I would like to express my sincere thanks and gratitude to my supervisor Dr. Cecilia Moloney for her guidance, constant encouragement and moral support which helped me in completing my programme. I also thank Dr. C. Moloney for the financial support she has provided me. I would like to express my deep gratitude and sincere thanks to Dr. Cecilia Moloney, Dr. Jim Sharp, Associate Dean, Faculty of Engineering for granting me leave in order to cope up with my most difficult situation in life to continue my programme. I will be grateful to them through my life for their act of kindness.

I would like to express my gratitude towards Dr. Seshadri, The Dean, Faculty of Engineering, MUN for his kind consideration and financial assistance. I would like to thank Dr. Morin for his guidelines in successfully presenting my thesis results and his suggestions on thesis contents. I also would like to thank Dr. Jeyasurya for his co-operation and constructive suggestions on thesis material organization. I also like to thank Dr. Venkateshan, Dr. Quicoe, and Dr. T.R. Chari for their encouragement and support.

Personally, I would like to thank Dr. Christopher Sharp, Associate Dean, School of Graduate Studies for granting me the leave specially near the end of my graduate programme and also for the financial assistance. I also thank all staff members, The School of Graduate Studies, MUN, for their pleasant and helpful nature.

I sincerely acknowledge Mr. Tony Parsons, and Marzia Zaman the former graduate students of Electrical Engineering, Faculty of Engineering, MUN for their resource material. I also would like to acknowledge C-CAE for their co-operation and support. I would also like to acknowledge all examiners of my thesis for their useful comments and suggestions.

I express my deep love to my mother, my brother Giri Prasad and my sisters Janaki Devi, Vijaya, Vidya who are always in my heart where ever I am. I acknowledge my thremendous love for my father who is watching me and blessing me through the doors of heaven. Finally, I acknowledge my thanks to Dr. Kasinadhuni Satyanarayana for his true love, support and encoragement. Thanks also to all who helped me in making this work a successful completion.

Dedication

With love to my father and mother.

Contents

Abstract	iii
Acknowledgement	v
Dedication	vi
Contents	vii
List of Figures	xi
List of Tables	xiv
List of Abbreviations and Symbols	xvii
1 Introduction	1
1.1 Motivation	1
1.2 Edge Detection	3
1.2.1 Edges as scene descriptors	3
1.2.2 Edge detection on noise-degraded images	3
1.3 Problem Definition	5
1.4 Research Methodology	6

1.4.1	Selection of test data	6
1.4.2	Experimental method	7
1.5	Thesis Outline	7
2	Literature Review	9
2.1	General	9
2.1.1	Conventional notation	10
2.1.2	Imaging systems	13
2.2	Speckle	14
2.2.1	Speckle origin	14
2.2.2	Speckle classification	15
2.2.3	Visual effect	16
2.2.4	Speckle statistical characteristics	18
2.3	Edge Detection Methods	21
2.3.1	Gradient edge detectors	21
2.3.2	Zero-crossing edge detectors	23
2.3.3	Ratio edge detectors	26
2.4	Speckle Specific Edge Detection Methods	27
2.4.1	Coefficient of Variation edge detector	28
2.4.2	Ratio of Averages (RoA)	29
2.4.3	Touzi Extended Ratio of Averages CFAR	31
2.4.4	Modified Ratio of Averages (MRoA)	33
2.4.5	Ratio and Gradient of Averages (RGoA)	34
2.5	Synthetic Aperture Radar Imaging	35
2.5.1	SAR imaging technology	35

2.5.2	Speckle noise in SAR images	36
2.5.3	SAR image data processing	38
2.5.4	Speckle noise models	41
2.6	Summary	43
3	Evaluation of Edge Detection Methods for Speckled Images	44
3.1	Introduction	44
3.2	Edge detector performance measures	44
3.2.1	Qualitative performance measures	45
3.2.2	Quantitative performance measures	46
3.3	Speckle noise simulation	48
3.4	Test data	51
3.4.1	Synthetic speckled images	51
3.4.2	Real airborne SAR images	55
3.5	Evaluation of edge detection methods	59
3.5.1	Evaluation using synthetic test images	59
3.6	Evaluation of edge detection methods for real airborne SAR images	69
4	Maximum Strength Edge Pruned Ratio of Averages Edge Detector	76
4.1	Introduction	76
4.2	The MSPRoA edge detection method	77
4.2.1	Terminology	77
4.2.2	The MSPRoA algorithm	78
4.2.3	Graphical illustration using 1-D signals	80
4.2.4	The effect of mask size (N)	85
4.2.5	The effect of correlation distance (d)	87

4.3	A 2-D example	88
5	Results and Discussion	94
5.1	Introduction	94
5.2	The MSPRoA on synthetic test images	95
5.2.1	Qualitative analysis of MSPRoA results on synthetic images	96
5.2.2	Quantitative analysis of MSPRoA results on synthetic images	102
5.3	The MSPRoA on airborne SAR images	105
5.3.1	Test Results	105
5.3.2	Analysis of MSPRoA test results on SAR Images	106
5.4	Discussion	114
5.4.1	Comparative study using synthetic test images	114
5.4.2	Study on the effect of mask size	122
5.4.3	Comparative study and analysis using SAR images	124
5.5	The MSPRoA edge tracking algorithm	131
5.6	Multi-scale MSPRoA edge detector	138
5.6.1	Multi-scale MSPRoA on synthetic test images	138
5.6.2	The Multi-scale MSPRoA on airborne SAR images	139
6	Conclusions and Future Studies	146
6.1	Conclusions	146
6.2	Future Studies	149
	References	151

List of Figures

2.1	One dimensional step edge	10
2.2	Edge detector processing window	11
2.3	A digital image grid	12
2.4	Speckle geometric phenomena	15
2.5	A laser speckle pattern visual effect	17
2.6	Speckle statistical characteristics	20
2.7	Gradient edge detection operators	22
2.8	Zero crossing Edge detector	24
2.9	Zero crossing edge detector templates	25
2.10	General schematic for ratio based edge detectors.	26
2.11	The schematic for Ratio of Averages (RoA) edge detector	29
2.12	The schematic for Touzi CFAR edge detector	32
2.13	The schematic for the Modified Ratio of Averages (MRoA).	33
2.14	A typical SAR amplitude image	37
2.15	Speckle noise model	42
3.1	Generation of synthetic speckle image	49
3.2	Synthetic test image <i>Strips</i> :	52
3.3	Synthetic test image <i>Ring</i> :	53

3.4	Synthetic test image <i>Combine</i> :	54
3.5	Real airborne SAR test image <i>Moderately Busy</i>	56
3.6	Real airborne SAR test image <i>Busy</i>	57
3.7	Real airborne SAR test image <i>Smooth</i>	58
3.8	Edge maps obtained for the <i>Strips</i> images:	61
3.9	Edge maps obtained for <i>Ring</i> images:	63
3.10	Edge maps obtained for <i>Combine</i> images:	65
3.11	Edge maps for SAR image <i>Moderately Busy</i> :	72
3.12	Edge maps for SAR image <i>Busy</i> :	73
3.13	Edge maps for SAR image <i>Smooth</i> :	74
3.14	Evaluation of edge detection methods for 16×16 SAR test samples:	75
4.1	A general pattern computing MSPRoA strength, $N = 5$, $d = 2$	77
4.2	Schematic of the MSPRoA edge detector.	79
4.3	Synthetic test image <i>Bars</i>	81
4.4	Illustration of the MSPRoA method using 1-D signals :	83
4.5	The effect of mask size on the MSPRoA method:	86
4.6	The effect of correlation distance d on the MSPRoA method	89
4.7	The MSPRoA edge detection test results on <i>Bars</i>	91
5.1	The MSPRoA test results on synthetic test image <i>Strips</i> :	97
5.2	The MSPRoA test results on synthetic test image <i>Ring</i> :	98
5.3	The MSPRoA test results on test image <i>Combine</i> :	99
5.4	The MSPRoA test results on SAR test image - <i>Fields</i> :	107
5.5	The MSPRoA test results on SAR test image <i>Busy</i> :	108
5.6	The MSPRoA test results on SAR test image <i>Highway</i> :	109

5.7	The MSPRoA test results on SAR test image <i>Industrial</i> :	112
5.8	The MSPRoA test results a comparative study using <i>Strips</i> :	119
5.9	The MSPRoA test results a comparative study using <i>Ring</i> :	120
5.10	The MSPRoA method a comparative analysis using <i>Combine</i> :	121
5.11	The MSPRoA results a comparative study on <i>Fields</i> :	126
5.12	The MSPRoA results comparative study for SAR <i>Busy</i> :	127
5.13	The MSPRoA test results a comparative study on <i>Highway</i>	128
5.14	The MSRoA results a comparative study for SAR <i>Industrial</i> :	130
5.15	The MSPRoA edge tracking algorithm test results for <i>Bars</i>	132
5.16	The MSPRoA edge tracking algorithm on <i>Bars</i>	134
5.17	The MSPRoA edge tracking algorithm	135
5.18	The MSPRoA edge tracking algorithm on <i>Combine</i>	136
5.19	Multi-scale MSPRoA results for <i>Balloon</i>	140
5.20	Multi-scale MSPRoA result for <i>Combine</i> :	141
5.21	The multi-scale MSPRoA on SAR test image - <i>Fields</i>	143
5.22	The multi-scale MSPRoA test results on SAR <i>Highway</i>	144
5.23	The multi-scale MSPRoA test results on SAR <i>Industrial</i> :	145

List of Tables

3.1	Standard ratio test for simulated speckle noise.	50
3.2	Quantitative performance measures on synthetic test images	67
3.3	Quantitative performance measures on synthetic test images	68
3.4	Evaluation of edge detection methods for real airborne SAR images	71
4.1	The MSPRoA performance evaluation for test image Bars	90
5.1	The MSPRoA edge detector quantitative evaluation measures	103
5.2	Optimizing edge detector quantitative performance measure W	115
5.3	Optimizing edge detector quantitative performance measure M	116
5.4	Optimizing edge detector quantitative performance measure A	117
5.5	The effect of nask size on MSPRoA edge detector	122

List of Important Abbreviations

AWGN	: Additive White Gaussian Noise
CFAR	: Constant False Alarm Rate
CoV	: Coefficient of Variation
CW	: Coontinuous Wave
LoG	: Laplacian of Gaussian
LR	: Likelihood Ratio
MMSE	: Minimum Mean Squared Estimate
MRoA	: Modified Ratio of Averages
MSPRoA	Maximum Strength edge Pruned Ratio of Averages
NMNV	: Non-stationary Mean Non-stationary Variance
Pd	: Probability of detection
PDF	: probability density function
Pfa	: Probability of False Alarm
PSF	: Point Spread Function
RGoA	: Ratio and Gradient Of Averages
RoA	: Ratio Of Averages
SAR	: Synthetic Aperture Radar
SNR	: Signal to Noise Ratio
SSNR	: Speckle Signal to Noise Ratio

List of Important Symbols

C	: "correct" edge factor
d	: Pruning (or correlation) distance
D	: edge pruning sub-window
$D(r)$: Maximum edge Strength
F	: "false" edge factor
G	: gradient magnitude
G_o	: gradient magnitude for the o th set of pair of the neighbourhoods
K	: edge tracking pixels
l	: edge tracking track length
L	: number of independent looks
M	: "missed" edge factor
N	: window size
R	: ratio magnitude
R_o	: ratio magnitude for the o th set of pair of the neighbourhoods
$R(r)$: MSPRoA edge strength magnitude
$R(o)$: MSPRoA edge strength orientation
T	: threshold
T_g	: gradient threshold
T_r	: ratio threshold
W	: "wrong" edge factor
h	: PSF of the imaging system
n	: noise process
$z(i, j)$: original or un-corrupted image at pixel (i, j)

$y(i, j)$: noisy image at pixel location (i, j)

Chapter 1

Introduction

1.1 Motivation

Edge detection methods for speckled images are important as these images are found in a variety of digital image processing application fields which use such images as laser, sonar, radar, synthetic aperture radar (SAR) and ultrasound, etc.

Speckle is a common phenomena in almost all images formed from coherent imaging systems and some non-coherent imaging systems [34] and may be responsible for causing hindrances to human or computer vision systems in extracting information from these images [3, 53]. Edge detection methods may help in conveying useful information on image contents. Since speckled images may contain useful information for applications such as remote sensing, medical imaging etc., there is a necessity for operators to extract accurate and precise information from these images.

It has been found that the speckle phenomena observed in images for coherent imaging systems cannot be avoided completely [10, 34]. Observed from the human vision point of view, speckle gives a granular texture appearance to images and may suppress true edge information or may trigger false edge points [3, 61, 82]. When analyzed statis-

tically speckle differs from other types of noise which are commonly observed in digital images such as additive white Gaussian noise (AWGN). Several existing edge detection methods used to extract information from non-coherently formed images are less suitable for use with coherent imaging images due to the nature of speckle noise found in these images [3, 82, 90]. In fact, most edge detection operators are best suited for use on noise-free images [77].

Various edge detection methods have been developed for use on noise-degraded images but these are better suited for AWGN environments. A literature search reveals that, although the nature and characteristics of speckle noise have been well studied and well established [34], the problem of detecting edges on speckled images has not been extensively studied. Relatively few edge detection methods have been proposed for use on speckled images [3, 23, 82, 90].

Edge detection methods that use ratios between pixel values tend to generate relatively better edge maps on speckled images when compared to gradient based methods that use differences between pixel values [3, 23, 82, 90]. However, ratio based methods generate thick edge edge maps and require edge thinning post processing [3, 69]. These methods may also require gradient information in order to generate precise edge maps on speckled images [3, 90]. The performance of these edge detectors may be poor on medium-to-low contrast images [89]. In this thesis, research has been conducted on edge detection methods for speckled images, motivated by the following goals:

- Extending available methods to improve accuracy.
- Satisfactory detection by extracting all true edge pixels.
- Low error rate by reducing false edge pixels information.
- High computational efficiency.

1.2 Edge Detection

1.2.1 Edges as scene descriptors

Edges in images are defined as transitions between regions having different intensities, textures, color or other image properties [77]. Several common types of edges separate regions with different intensities. The edges may help in describing scene contents by giving definition to underlying image objects. Achieving the goal of edge detection may simplify computations in computer vision algorithms such as segmentation, classification and pattern or object recognition.

When analyzing complex scenes it can be often useful to simplify the amount of data to be processed by discarding information regarding absolute gray levels and only keeping a record of places where changes occur in the image. Several modern theories rely on pre-processing images with detection operators before image matching and object recognition. For these reasons edge detection is often considered to be one of the first stages in many image processing procedures [63, 65].

1.2.2 Edge detection on noise-degraded images

The goal of edge detection for noise-degraded images may be achieved by following two different approaches. They are:

- Direct methods: Use of edge detection operators on images available for use.
- Indirect methods: Use of edge detection operators on pre-processed images.

The direct methods of edge detection achieve the goal of edge detection by applying edge detection operators directly to an image. These methods do not use pre-processing operations such as noise filtering, image enhancement etc. In the case of noise-degraded

images, these methods require edge detection operators which have been designed according to a model of the interfering noise. *A priori* knowledge about the interfering noise may help in selecting an appropriate edge detection operator in this case. The design of new edge detection operator also benefits from knowledge of the nature and characteristics of interfering noise. These methods provide direct solutions to the problem of edge detection by reducing computational costs required for image enhancement or noise smoothing pre-processing operations.

Indirect edge detection methods usually include one or more pre-processing operations before the actual edge detection is performed. Pre-processing may include image enhancement, edge preserving noise smoothing or filtering operations. An edge detection operator is then applied to the pre-processed image. *A priori* knowledge of the characteristics of any interfering noise is required in this case, for selecting the filter to be used for noise smoothing. Since edge detection is performed on noise filtered images, the use of gradient edge detection methods may give better performance results. But pre-processing operations may generate additional problems in this case such as edge blurring, smoothing of fine details in the course of pre processing operations, etc. The overall performance of the edge detection in this case depends on both the performance of the pre-processing operators and the edge detection operator.

In this thesis, edge detection methods for speckled images that use direct methods without pre-processing operations are discussed. Concepts involved in the design of new edge detection operators which improve the performance of the existing edge detection methods are studied.

1.3 Problem Definition

Speckle is usually characterized as multiplicatively signal-dependent and may be spatially highly correlated [34]. Speckle varies with underlying image intensity i.e. the speckle is significant in high intensity homogeneous regions compared to low intensity homogeneous regions. As a result, the signal to noise ratio (SNR) of speckled images may be low and these images may suffer from poor contrast ratios as well [17, 23, 54]. All these properties make automated extraction of edge information from speckled images a difficult task to accomplish.

Gradient edge detection methods which are based on differences between pixel values give inconsistent estimates regarding true edge pixels due to the signal dependent nature of speckle noise. Gradient methods can provide computationally inexpensive solutions to the problem of edge detection on noise-free images. But these methods have been shown to generate spurious edges and thick edge maps when used on speckled images [3, 69, 91].

Zero-crossing edge detectors applied to speckled images have been shown to generate thin and localized edge maps but also to generate a number of spurious edges [3]. The main disadvantage with these methods is that they are insensitive to the edge magnitude strength [40]. Other methods using ratios between pixel values tend to cancel out the multiplicative noise effect of the speckle in the speckled images and to generate meaningful edge maps on these images [3, 82]. Evaluations of edge detection methods for speckled images have shown that ratio based methods perform better than gradient based methods [69, 91, 32].

However, existing ratio based methods also tend to generate thick edge maps. Post-processing edge thinning operators are required in order to generate precise edge maps.

These methods also use gradient edge strength measures for generating well defined and meaningful edge maps [3, 91]. These methods trade off the number of spurious edge pixels generated in homogeneous regions and the number of correct edge pixels [90]. Such edge detectors used with large mask sizes can be successful in suppressing the spurious edges in homogeneous regions, but also generate thick edge maps. On the other hand, small mask sizes are successful in extracting fine details and also give thin and precise edge maps but generate number of spurious edges [32, 69]. Extracting information regarding the fine structures in images is also another problem with existing speckle specific edge detection methods [69].

1.4 Research Methodology

1.4.1 Selection of test data

Test data were selected to include a variety of test images over a range from simple 1-D signals to real airborne synthetic aperture radar (SAR) amplitude images. As a simple test category 1-D signals are selected which have gray level values between 0-255 and which include low intensity homogeneous regions, high intensity homogeneous regions and edge pixels. In a second category, 2-D simulated speckled images with 256 gray levels varying between 0-255 are considered. Test examples in this case include computer generated patterns and real outdoor scenes. In a third category, SAR images extracted from a data set are used with the permission of Canada Center for Remote Sensing (CCRS), Ottawa, Canada. Test images consisting of a variety of scene contents such as *woods, farm land, city, highway, industrial* etc. are selected as test examples in this category.

1.4.2 Experimental method

First, existing edge detection methods used for edge detection on speckled images are studied. Then the performance of different edge detection methods is evaluated using the 1-D signals and 2-D synthetic test images. Since the original test images are noise-free with sharp edges the *Sobel* operator [77] is used to generate edge maps representing ideal edge maps. Edge maps on the corresponding simulated speckled images are obtained using several existing edge detection methods representing actual edge maps. Quantitative and qualitative evaluation of existing edge detection methods is made by comparing the corresponding ideal edge maps and the actual edge maps. This work follows the the measures proposed by Zaman and Moloney [89] which they used in the study and analyze of edge preserving noise smoothing digital filters. A similar evaluation of existing edge detection methods is also made using real airborne SAR images to investigate the suitability of these methods on real data sets. The means of improving the existing edge detection methods for extracting accurate and precise edge maps for speckled images are investigated.

1.5 Thesis Outline

This thesis is arranged into six chapters. In Chapter 2 a review of relevant literature is conducted. The nature and characteristics of speckle noise are reviewed. Public domain edge detection methods in general and speckle specific edge detection methods in particular are reviewed. Introductory concepts used in SAR imaging systems are briefly outlined.

In Chapter 3 an evaluation of existing edge detection methods for speckled images is performed using qualitative and quantitative performance measures. The performance

of these methods on real airborne SAR images is evaluated.

A ratio edge detector based on maximum strength edge pruning (MSPRoA) [33] for extracting accurate and precise edge maps on speckled images is proposed in Chapter 4. The MSPRoA algorithm and test results using 1-D test signals are presented.

The MSPRoA edge detection test results using images both synthetic 2-D and real airborne SAR images are presented in Chapter 5. The performance of MSPRoA edge detector on a variety of test images is evaluated using qualitative and quantitative methods. A simple and fast MSPRoA edge tracking algorithm to improve visual quality of the MSPRoA edge maps is proposed. The use of multi-scale MSPRoA method for extracting information at both macro and micro levels on speckled images is suggested. The multi-scale MSPRoA method performance is verified using synthetic and real SAR images.

In Chapter 6, conclusions and recommendations for future studies are presented.

Chapter 2

Literature Review

2.1 General

This chapter presents a literature survey of several topics related to this thesis notably: edge detection methods, the nature and characteristics of speckle noise and SAR imaging systems. The nature of speckle noise, including its visual effect and statistical characteristics are briefly introduced. Edge detection methods, in general, and in particular methods that are better suited for use on speckled images are reviewed. Previous speckle-specific edge detection methods and their algorithms are introduced. SAR imaging technology, SAR data processing, speckling effects observed in SAR images and related background information are provided. Speckle noise models for simulating SAR speckle using radar signals model are also reviewed.

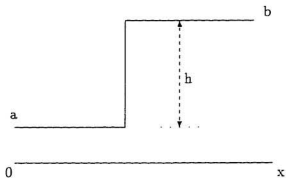


Figure 2.1: One dimensional step edge

2.1.1 Conventional notation

- **Edge**

The most common type of edge in images separates regions with different intensity levels. Figure 2.1.1 shows a one dimensional step edge in images. The step edge is characterized by its height h indicating the difference between two intensity levels of values a and b respectively. An edge exists if the absolute difference between two levels a and b is greater than a pre-set value which is considered to be the threshold value separating edge and non-edge magnitudes and hence detecting difference between edge and non-edge pixels.

- **Processing window W**

Edge operators in general select a set of pixels as a processing window or mask which is used for the computation of edge strength values. The mask size $m \times n$ determines the number of rows (m) and columns (n) of the processing window. If a processing window contains an equal number of rows and columns it may

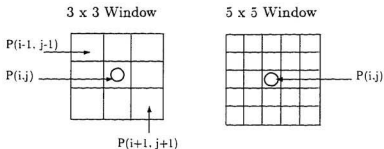


Figure 2.2: Edge detector processing window

be represented by a mask size N (indicating that the processing window of size $N \times N$, where N is odd). Figure 2.2 shows two conventional processing windows for mask size $N = 3$ and $N = 5$ with the center pixel $P(i, j)$ indicated by a circle. In this thesis processing window (or window) or mask represents square matrix of pixels as shown in Figure 2.2.

- **Digital image**

Figure 2.3 shows a digital image of size $M \times N$ pixels arranged into M rows and N columns. Pixel $P(0, 0)$ located at top left corner and pixel $P(M - 1, N - 1)$ located at the bottom right corner. The Figure 2.3 also shows a pixel of interest $P(i, j)$ (located at i row and j column indicated by the circle) where the edge strength value is to be measured applying a 3×3 window. The digital images used in this thesis are either gray scale image (intensity values represented by 8-bits or levels $0 - 255$), or binary (represented by two levels-black and white) to represent edge maps.

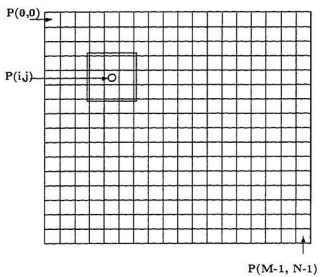


Figure 2.3: A digital image grid

2.1.2 Imaging systems

Imaging systems can be broadly classified into coherent and incoherent systems based on the illumination source used in image formation. Differences exist between coherent and incoherent imaging in the way images are formed. Historically, images have been performed with incoherent illumination [4] such as sunlight. A variety of optical and electromagnetic (EM) instruments which require coherent illumination for their applications have been developed. The invention of the laser in the early 1960's opened new horizons for imaging systems using coherent illumination. Holographic imaging is a two step image processing that uses coherent illumination. Radar systems obtain images using coherent processing. Lasers used for illumination purposes use highly coherent light.

Incoherent imaging systems are linear in intensity and the phase information associated with the object being illuminated is not retained in any way. In these systems all possible phases are represented. The human vision system and photographic systems are most common examples of imaging systems that use incoherent processing.

Coherent systems are linear in complex intensity and the phase information associated with the object is retained. These imaging systems have illumination energy in which phases are aligned. The process becomes more complicated when images are formed using coherent and reflected energy. With reflected energy signal there is a second problem associated with the phase differences that are introduced into the reflected beam due to the surface roughness of the object being illuminated. These parameters in coherent imaging systems give rise to noise patterns called *speckle* which may degrade the images formed by the system. This thesis addresses images obtained using synthetic aperture radar (SAR) which are formed using coherent processing and are further discussed in section 2.5.

2.2 Speckle

2.2.1 Speckle origin

The operation of the first HeNe laser in 1960 revealed a peculiar granular pattern called *laser speckle* phenomenon [34]. It was found that the speckle patterns are produced as a result of the scattering of coherent light from surfaces which are rough on the scale of optical wave lengths (5×10^{-7} meters).

When objects are viewed in highly coherent continuous wave (CW) laser light the response observed at a distant point consists of many coherent components each arising from a different microscopic element of the surface being illuminated. The distances traveled by these coherent components may differ by several or many wavelengths if the surface is truly rough. The resultant field will therefore consists of contributions from several component waves which are in and out of phase, although coherent, thus resulting in the appearance of a granular pattern.

If interference at any point is highly constructive the resultant speckle pattern consists of bright spots. If the interferences are highly destructive then the resultant pattern consists of dark spots. Overall the *speckle* consists of random spots bright and dark intensities and, of intensities in between these two extremes. If the observation point is shifted in space, the resultant speckle pattern will also change due to a new set of components contributing to the resultant field.

A literature search shows that direct analogies of laser speckle are found in coherent imaging such as radar astronomy, synthetic aperture radar (SAR) and acoustical imagery [34]. In addition, speckle-like patterns are also observed in radio wave propagation, temporal characteristics of incoherent light, the theory of narrow band electrical noise, ultrasound and general theory of random spectral analysis [10]. The term *speckle* has

now taken on a far broader sense than when it was first introduced as *laser speckle*.

2.2.2 Speckle classification

It is convenient to classify speckle patterns into two groups, objective and subjective speckle. The scattering of a rough surface illuminated by a coherent light source is known as objective speckle. A part of objective speckle can be observed by holding a screen in front of the object being illuminated. Briefly, objective speckle is speckle observed in free-space geometry. Subjective speckle patterns can be observed by focusing the scattering of a rough surface using a lens system as shown in Figure 2.4. In other

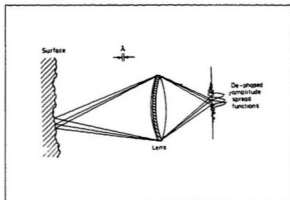


Figure 2.4: Speckle geometric phenomena

words, subjective speckle is objective speckle obtained by considering the lens pupil as the scattering surface. Subjective speckle is different in that an image of the object is formed by using lens system.

It may be considered that there is no difference between objective and subjective

speckle but they are speckle patterns at different scales, i.e they will have different visual patterns appearance. The speckle observed in imaging systems are examples of subjective speckle patterns.

2.2.3 Visual effect

Figure 2.5 shows speckle patterns produced from a reflected surface such as paper (Goodman [34]). Dennis Gabor, who received the 1971 Nobel prize in physics for his invention of holography says that the speckle is not really noise but, it is information which we do not want i.e the information on the microscopic unevenness of the paper in which we may not be interested.

The speckle patterns can be used for beneficial purposes in applications such as meteorology, astronomy, stellar interferometry etc. A collection of engineering uses of the speckle can be found in [25, 26]. The speckle patterns are used in measuring surface roughness, non-destructive testing of finished mechanical components, detection of cracks in aircraft wings, detection of distortion in engine bearings etc. An extensive review on use of speckles in meteorology can be found in [27]. Another important area covers applications in astronomy and stellar interferometry. Speckles are used for measuring the diameters of asteroids and planets [28], solar granulation [29], angular separation and position angle of binary stars [30].

However, speckle is most commonly treated as noise or unwanted disturbance in image processing and computer vision application as it obscures observable details in the underlying images. It is seen from Figure 2.5, that speckle patterns consists of random bright and dark patches of random widths distributed all over in a totally chaotic manner. Though there may not be much information that image processing and computer vision applications from a surface such as plain paper (no intensity changes

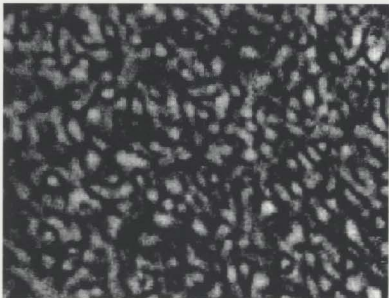


Figure 2.5: A laser speckle pattern visual effect
Copied from *Laser speckle and related phenomena*,
J.W. Goodman and J.C Dainty [34], page. 10.

or no objects to register, etc.) but the speckles give impression that there may be some useful information. It may be difficult or may be impossible in some cases even for the human vision systems to recognize fine detailed information in speckled images due to the visual effects created by the speckle noise.

2.2.4 Speckle statistical characteristics

The statistical characteristics of speckle patterns have been well studied and established [34, 10]. Goodman derived the first and second order statistical characteristics of laser speckle patterns [34]. Since the derivations are lengthy and outside the scope of this thesis, only a summary of these results is presented here.

The complex amplitude scattered light at a distance observation point in space is given by the sum of amplitudes of the contributions from each point source on the scattering surface (Figure 2.4). Assuming that the number N of elementary contributions a_k is extremely large, i.e. $N \rightarrow \infty$, Goodman derived the joint probability density function (*PDF*) $p_{r,i}$ of the real (A_r) and imaginary (A_i) parts of the speckle patterns as.

$$p_{r,i}(A_r, A_i) = \frac{1}{2\pi\sigma^2} \exp\left(-\frac{[A_r]^2 + [A_i]^2}{2\sigma^2}\right) \quad (2.1)$$

$$\sigma^2 = \lim_{N \rightarrow \infty} \frac{1}{N} \sum_{k=1}^N \frac{\langle |a_k|^2 \rangle}{2} \quad (2.2)$$

Where $\langle a_k \rangle$ is ensemble average of a_k elementary contributions. The *PDF* $p_{r,i}$ is commonly known as a circularly Gaussian density function since contours of constant *pdf* are the circles in complex plane.

The quantity that is frequently considered in the field of digital image processing is the intensity of the speckle patterns. Goodman derived the equation for the marginal

PDF of the speckle intensity alone $p_I(I)$ as:

$$p_I(I) = \int_{-\pi}^{\pi} p_{I,\theta}(I, \theta) d\theta = \begin{cases} \frac{1}{2\sigma^2} \exp(-\frac{I}{2\sigma^2}) & I \geq 0 \\ 0 & \text{otherwise} \end{cases} \quad (2.3)$$

The PDF of the intensity $P(I)$ which is greater than some set threshold value I is expressed as:

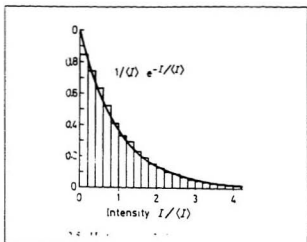
$$P(I) = \exp(-\frac{I}{\langle I \rangle}) \quad (2.4)$$

In general, speckle consists of sum of two or more polarised speckle patterns. Thus the total intensity of the irradiance I may be composed of N speckled patterns.

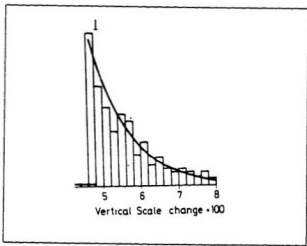
$$I = \sum_{k=1}^N I(k) \quad (2.5)$$

where $I(k) = |A_r(k)^2 + A_i(k)^2|$. Thus speckle patterns may also express correlations between underlying intensity fields.

Goodman deduced that speckle patterns obey negative exponential statistics. His results were later confirmed experimentally by many other researchers [10, 67]. McKechnie [67] who took 23,000 measurements reported in his experiments that speckle exhibits negative exponential characteristics. Figure 2.6(a) shows Goodman's theoretical plot of speckle characteristics. Figure 2.6(b) shows McKechnie experimental results showing speckle characteristics. Figure 2.6(a) and (b) confirm that speckle intensity exhibits negative exponential characteristics.



(a)



(b)

Figure 2.6: Speckle statistical characteristics

(a) Goodman theoretical plot; (b) McKechnie experiments. (Copied from *Laser speckle and related phenomena*, J.W. Goodman and J.C. Dainty [34], pp. 19.

2.3 Edge Detection Methods

2.3.1 Gradient edge detectors

Gradient edge detectors in general calculate edge strength value based on differences between pixel values. These operators use edge templates, which are processing windows but each element in the window is assigned a value which is different for different operators. At each pixel $P(i, j)$ in the input image, the edge strength magnitude $A(i, j)$ is calculated as per the edge operator algorithm applying edge template. A pixel $P(i, j)$ is classified as an edge pixel if the edge strength value $A(i, j)$ is greater than a pre-set threshold value. The image defined by the $A(i, j)$ values is called the edge strength map while the corresponding thresholded version is called edge map $E(i, j)$ which is a binary image indicating edge and non-edge pixel location by 1's and 0's respectively. If edge map is obtained from noise-free image then it is referred as ideal edge map indicating ideal edge pixel locations. If edge map is obtained on noise corrupted image then, it is referred as actual edge map which indicates actual edge pixel locations in the detected edge map.

Different gradient edge operators based on edge templates have been suggested by researchers in the past such as Sobel, Robert, Prewitt, Kirsch etc. [77]. Figure 2.7 (a) and (b) shows edge templates for Sobel and Prewitt operators, respectively. According to these methods an edge strength magnitude is calculated by applying the appropriate row and column gradient masks at each input image pixel. The square root of the sum of row and column gradient masks computed and is considered as the overall edge strength measure. An edge strength map so obtained is thresholded to separate the edge pixels from the non-edge pixels.

That is, the Sobel operator measures edge strength value by applying the row and

Row gradient

1	0	-1
2	0	-2
1	0	-1

Column gradient

-1	-2	-1
0	0	0
1	2	1

(a) Sobel operator

1	0	-1
1	0	-1
1	0	-1

-1	-1	-1
0	0	0
1	1	1

(b) Prewitt operator.

Figure 2.7: Gradient edge detection operators

column Sobel edge templates (Figure 2.7(a)) at each pixel $P(i, j)$ in the input image. The Sobel operator calculates the overall edge strength value at each pixel $P(i, j)$ using:

$$E(i, j) = \sqrt{[G_R(i, j)]^2 + [G_C(i, j)]^2} \quad (2.6)$$

where G_R and G_C are row and column edge strength magnitudes, respectively. If $L1$ and $L2$ are left and right sum and differences of pixel intensity values of the pixel $P(i, j)$. Sobel operator calculates G_R and G_C edge strength measures using the following set of equations.

Row gradient:

$$G_R(i, j) = \frac{1}{K+2}[L1 - L2] \quad (2.7)$$

$$L1 = P(i-1, j) + K \times P(i, j+1) + P(i+1, j+1)$$

$$L2 = P(i-1, j-1) + K \times P(i, j-1) + P(i+1, j-1)$$

Column gradient:

$$G_C(i, j) = \frac{1}{K+2}[L1 - L2] \quad (2.8)$$

$$L1 = P(i-1, j-1) + K \times P(i-1, j) + P(i-1, j+1)$$

$$L2 = P(i+1, j-1) + K \times P(i+1, j) + P(i+1, j+1)$$

Similarly, an edge strength map can be obtained using the Prewitt operator edge templates shown in Figure 2.7(a) and substituting $k = 1$ in the above set of equations. There exist many different operators based on the computation of gradient edge strength values, but most of them use similar techniques based on local gradient information [77]. Gradient edge detectors are best suited for applications on noise-free images.

2.3.2 Zero-crossing edge detectors

The concepts involved in zero-crossing edge detector can be best described by considering a simple one-dimensional continuous step edge as shown in Figure 2.8(a).

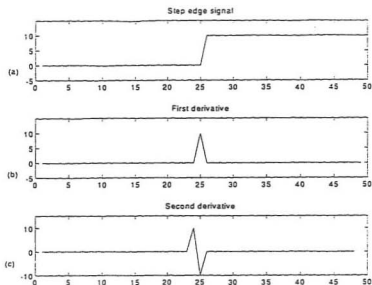


Figure 2.8: Zero crossing Edge detector

(a) One-dimensional analog step edge; (b) The first derivative measured on (a); (c) The second derivative measured on (a).

Figure 2.8(b) shows the first derivative of the step edge which gives local maximum at edge locations. Figure 2.8(c) shows the second derivative of the signal 2.8(a) which gives zero crossings at the places where the first derivative maxima are found. A zero crossing edge detector calculates edge pixels at locations where the spatial gradient finds its maximum values i.e. a pixel is marked as an edge pixel if there is a “zero” crossing of the second derivatives at that pixel [77]. The generalization of the zero-crossing edge detector in 1-D domain leads to the Laplacian operator in two dimensional domain.

Figure 2.9(a) shows two common 3×3 Laplacian masks used for computing the

	1	
1	-4	1
	1	

1	1	1
1	-8	1
1	1	1

 $\frac{1}{3}$

Figure 2.9: Zero crossing edge detector templates
 (a) A 3×3 masks employed in calculating 2-D Laplacian

a	b	a
b	e	b
a	b	a

Figure 2.9(b) General pattern of a 3×3 mask used in computing a 2-D digital Laplacian. The constraints are: (i) $e = -(4a + 4b)$ and (ii) $2a + b = 1$ [77].

2-D Laplacian operator. A Laplacian operator detects edges by convolving an input image with the Laplacian mask and using a threshold value to separate edge pixels from non-edge pixels.

Zero crossing edge detectors can be used to generate edge maps with sub-pixel accuracy and are successful in generating good localized edge maps. But one problem with these operators is that they are insensitive to the edge magnitude. The masks used for computing digital Laplacian are not necessarily optimal. Various 3×3 masks can correctly compute a digital Laplacian but may have different performance characteristics under different noise environments.

When applied on speckled images zero-crossing operators have been found to be successful in generating thin and localized edge maps [3]. However, the edge maps also

included spurious edges giving poor definitions compared to an ideal edge map when applied on speckled images [3, 89].

2.3.3 Ratio edge detectors

It has been found that edge detection methods using ratios between pixel values tend to cancel out the effect of multiplicative noise present in speckled images and to generate better edge maps when compared to the gradient methods for such images [2, 23, 82]. Figure 2.10 shows a schematic used to describe ratio based methods.

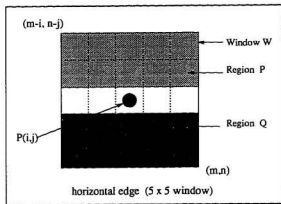


Figure 2.10: General schematic for ratio based edge detectors.

The processing window of a selected size is divided into two non-overlapping regions P and Q along one of the possible edge orientation α . The average pixel intensity P_α and Q_α are calculated for each of the two regions. The minimum of the two ratio of averages (P_α/Q_α) , (Q_α/P_α) is considered as edge strength measure R_α for the selected

edge direction ϕ . The ratio-of-averages edge strength value is calculated for each of the selected edge directions. The minimum of all the ratio-of-averages R_e is considered as the overall edge strength measure of the image pixel under consideration.

If the area which includes regions P and Q is homogeneous, the ratio-of-averages calculated for these regions will be approximately equal to unity which indicates a non-edge condition. If regions P and Q represent different homogeneous areas, then the ratio-of-averages measured will have a value other than 1, based on the respective relative average pixel intensity value over regions P and Q . A pre-set ratio threshold value T_r can be used to separate edge and non-edge pixels.

For speckled images, ratio based edge detectors perform better than gradient or zero-crossing edge detectors [2, 23, 82, 90]. However, these methods trade-off the number of false edge pixels and the number of correctly detected edge pixels when compared with their corresponding edge maps obtained on noise-free images. These methods also generate thick edge maps.

2.4 Speckle Specific Edge Detection Methods

In this section several existing speckled specific edge detection methods are reviewed in terms of their algorithms, advantages and disadvantages. The following edge detection algorithms are reviewed:

- Coefficient of Variation (CoV) [82] edge detector.
- Ratio of Averages [3] edge detector.
- Touzi Extended Ratio of Averages [82] edge detector.
- Modified Ratio of Averages (MRoA) [90] edge detector.

- Ratio and Gradient of Averages (RGoA) [90] edge detector.

2.4.1 Coefficient of Variation edge detector

Touzi [82] proposed the coefficient of variation (CoV) edge detector for speckled images and used radar images as his application example. According to the statistical nature of speckle, outlined above in section 2.2.4, the ratio of local standard deviation to mean in homogeneous areas does not depend on local mean power. Touzi used this fact and defined coefficient of variation (CoV) edge detector for use on radar images.

An estimate of the CoV is computed for an image pixel of interest by selecting a window surrounding the pixel of interest and using the standard deviation (σ) and mean (μ) of the pixels in the selected window. According to Touzi, the CoV edge strength value is measured using:

$$\sigma/\mu = \frac{\sqrt{\text{var}(x)}}{E(x)} \quad (2.9)$$

where, values σ and μ are computed using,

$$\mu = \frac{1}{N} \sum_{i=1}^N y_i \quad (2.10)$$

$$\sigma^2 = \frac{1}{N-1} \sum_{i=1}^N (y_i - \mu)^2 \quad (2.11)$$

For practical applications, value of σ/μ is approximately equal to $\sqrt{(1/L)}$ over a homogeneous areas, where L is the number of independent looks used in forming the radar image. This value could be higher over edge areas. Hence a threshold value is set using approximation $T = \sqrt{\frac{1}{L}} + \epsilon$, where ϵ is very small quantity. Image pixel $P(i, j)$ is labeled as an edge pixel if the edge strength value is greater than the pre-set threshold value. Hence, the CoV edge detector detected edges if:

$$\sigma/\mu \geq \sqrt{(1/L)} + \epsilon \quad (2.12)$$

All other pixels are classified as non-edge pixels. The larger the σ/μ value the more likely that the pixel is an edge pixel.

2.4.2 Ratio of Averages (RoA)

Bovik [3] suggested the simple Ratio of Averages method for detecting edges in speckled images by considering horizontal and vertical edge orientations. Figure 2.11 shows a schematic diagram of Bovik's Ratio of Averages (RoA) edge detector. According to the RoA edge detector, a selected neighborhood (window W) surrounding the image pixel of interest $P(i, j)$ is divided into two non-overlapping regions P and Q (Figure 2.11). The average intensity value of the pixels in the two regions P and Q are calculated as $R(i, j)$ and $L(i, j)$, respectively.

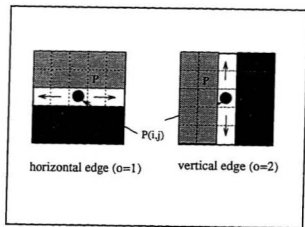


Figure 2.11: The schematic for Ratio of Averages (RoA) edge detector

The RoA edge strength value for horizontal and vertical edge orientations are calcu-

lated using:

$$H(i, j) = \max[R(i, j)/L(i, j), L(i, j)/R(i, j)] \quad (2.13)$$

$$V(i, j) = \max[R(i, j)/L(i, j), L(i, j)/R(i, j)] \quad (2.14)$$

The overall edge strength magnitude is calculated as,

$$R(i, j) = \sqrt{H(i, j)^2 + V(i, j)^2} \quad (2.15)$$

Edge strength map so obtained can be thresholded to separate edge pixels from non-edge pixels. That is, an image pixel $P(i, j)$ is classified as an edge pixel if $R(i, j) > T$, otherwise it is classified as a non-edge pixel.

Bovik noted that the conventional RoA method is successful in detecting edges in speckled images since the method is invariant to intensity changes [3]. However, the RoA method generates thick edge maps. Bovik also showed via his experimental results that the Laplacian of Gaussian (LoG) operator can be successful in generating good localized edge map for speckled images. However, the LoG method generates a number of spurious edge pixels.

According to Bovik, the advantages of RoA method are the disadvantages of LoG method and vice versa. The RoA method gives an optimal edge map for speckled images but, generates thick and ambiguous edge maps, where as LoG generates thin and localized edge maps but results in number of erraneous edges. He suggested that these two edge detectors be used in combination to give better results on speckled images. He used the RoA method in combination with the LoG method by combining the respective two edge maps using a logical AND operator.

Bovik demonstrated that the use of RoA and LoG methods in combination is successful in generating meaningful edge maps on speckled images. But the RoA method

uses only horizontal and vertical edge orientations which lead to a poor quantization of the possible edge orientations. A good edge detector should include information on all possible edge orientations for extracting as many true edge pixels as possible [82].

2.4.3 Touzi Extended Ratio of Averages CFAR

Touzi *et. al.* [82] also proposed a statistical and geometrical edge detector for SAR images considering ratios between pixel values. Their proposed edge detector uses contrast ratio C_r between two homogeneous regions in a selected neighborhood. They suggested that in order to obtain better performance results an edge detector must be applied in all possible directions. Accordingly, Touzi *et. al.* considered four main edge orientations, namely, *horizontal*, *vertical*, *left slanted* and *right slanted*. For each of these edge directions, a window centered at given pixel $P(i, j)$ is divided into two contiguous non-overlapping regions P and Q . Figure 2.12 shows a schematic used to describe the Touzi *et. al.* edge detector.

Touzi *et. al.* proposed extended ratio of averages edge detector which uses constant false alarm rate (CFAR) concept. A contrast ratio C_r is used to define edge and non-edge conditions. A contrast ratio of $C_r \approx 1$ is defined for homogeneous regions. For non-homogeneous regions contrast ratio value is determined using:

$$C_r = \max(P_o/Q_o, Q_o/P_o), \quad o=1, \dots, 4. \quad (2.16)$$

where P_o and Q_o are average pixel intensity values of two selected regions in the edge direction o . The conditional probability of detection within boundaries between two homogeneous regions having contrast ratio C_r , for a given threshold value T , is calculated using:

$$Pd(T, C_r) = \text{Prob}(r < T \mid C_r) = \int_0^T p(r \mid C_r) dr \quad (2.17)$$

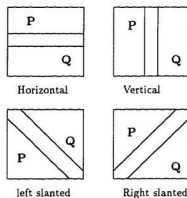


Figure 2.12: The schematic for Touzi CFAR edge detector

Touzi *et. al* defined the probability of false alarm (Pfa) as the probability that a pixel of a homogeneous area is detected as an edge pixel, and hence,

$$Pfa(T) = Pd(T, 1) \quad (2.18)$$

Touzi *et. al* also proposed a multi-scale CFAR detector using increasing mask sizes and different threshold values for each mask size. Touzi *et. al* obtained edge maps using different mask sizes ($3 \times 3, 5 \times 5, 7 \times 7, 9 \times 9$) and combined these edge maps using logical OR operator thus producing final edge maps for speckled images. Touzi *et. al* suggested that the multi-scale CFAR edge detector be used for extracting fine and large object detail on radar images. Touzi *et. al* CFAR method also used edge thinning post-processing in order to produce thin and precise edge maps.

2.4.4 Modified Ratio of Averages (MRoA)

Zaman and Moloney [90] modified the Bovik RoA method by taking all four edge orientations into account, namely *horizontal*, *vertical*, *left slanted* and *right slanted*. In their Modified Ratio of Averages (orientations) edge detector. Figure 2.13 shows schematic of the MRoA edge detection method.

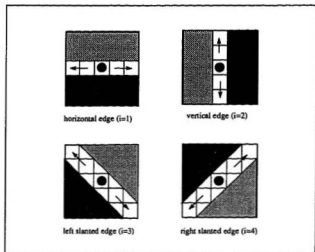


Figure 2.13: The schematic for the Modified Ratio of Averages (MRoA).

The processing window W of a given mask size N centered around the image pixel of interest $P(i, j)$ is divided into two non-overlapping regions for each of the four edge directions. Ratio of averages edge strength value is calculated for each edge of the edge orientation o using:

$$R_o = \min(P_o/Q_o, Q_o/P_o); \quad o=1, \dots, 4 \quad (2.19)$$

where P_o and Q_o are the averages of the pixel intensity values in the two non-overlapping regions in direction o . The overall edge strength value is measured using:

$$R = \min(R_1, R_2, R_3, R_4) \quad (2.20)$$

An edge strength map so obtained is thresholded to separate edge pixels from non-edge pixels. If the ratio edge strength value R at any pixel is less than the pre-set ratio-threshold value T_r then the pixel is classified as an edge pixel. All other pixels are labeled as non-edge pixels.

The Zaman and Moloney MRoA edge detection method can detect accurate edge maps including a number of correct edge pixels which may be missed by the Bovik RoA which uses only the horizontal and vertical edge directions. However, the edge maps generated using the MRoA method are thick and required edge thinning post processing operations to produce precise edge maps.

2.4.5 Ratio and Gradient of Averages (RGoA)

Zaman and Moloney further improved the MRoA edge detector by including gradient edge strength information in extracting correct edge pixels information from speckled images. According to them, the MRoA method detects more spurious edges in dark areas compared to bright areas even if the contrast ratio is held constant. This becomes a problem if edges have to be detected from both bright and dark regions in the same image, as is frequently required. Zaman and Moloney hence suggested that gradient edge strength information be included in calculating edge strength and hence developed the Ratio and Gradient of Averages (RGoA) edge detector [90].

The RGoA edge detector calculates edge strength measure in terms of both *ratio* and *gradient* edge strengths. The Schematic of Figure 2.13 also applies to the RGoA edge

detection method. The ratio edge strength value is measured using the MRoA method as explained in the previous section. The *gradient* edge strength value is calculated for each of the four directions of Figure 2.13 using:

$$G_o = \text{abs}(P_o - Q_o), \quad o=1, \dots, 4. \quad (2.21)$$

The overall gradient edge strength magnitude is calculated as:

$$G = \max(G_o), \quad o=1, \dots, 4. \quad (2.22)$$

The overall edge map is obtained by combining edge maps extracted based on ratio and gradient edge strength measures using the logical OR operation. The RGoA method detects edge pixels if:

$$R < T_r \quad \text{OR} \quad G > T_g \quad (2.23)$$

where T_r and T_g are pre-set ratio and gradient threshold values, respectively.

The RGoA method can successfully extract true edge pixels giving with better results than the MRoA edge detection method. The edge pixels that are detected using MRoA method are also included in the edge maps obtained using the RGoA method because the later method is an extension of the first method with the addition of gradient edge strength information. The RGoA method also require edge thinning post-processing to generate thin and precise edge maps on speckled images.

2.5 Synthetic Aperture Radar Imaging

2.5.1 SAR imaging technology

RADAR is an all-weather day/night sensor and has been used for a wide variety of surveillance applications since World War II. Radars detect targets by sending pulses

of radio waves toward them, and detecting any reflected energy. Imaging radars use a moving platform, with the radar antenna pointed perpendicular to the direction of the platform motion, to provide a second dimension (azimuth) and thereby build up a two-dimensional strip image. Imaging radars have been used since 1960 in military and civilian applications all over the world. An advanced signal processing version of these radars, known as synthetic aperture radar (SAR) provides 2-D imagery.

Synthetic Aperture Radar (SAR) is an airborne or space borne imaging system that uses coherent processing of returned radar signals. SAR provides an efficient means for better understanding and monitoring of the Earth environment and resources. SAR is a microwave instrument that sends pulsed signals towards targets and processes any reflected pulses from the targets. Optical satellite based remote sensing depends on sunlight to illuminate targets. Hence their performance is limited to the presence of clouds, haze, smoke and darkness. But SAR transmits and receives signals through clouds, haze, smoke and darkness providing an all-weather all-time means to obtain high quality images of the Earth from remotely observed platforms.

SAR images are increasingly used in remote sensing applications such as geology, mining, fishing, farming, forestry, sea ice mapping and hazardous monitoring [78, 5, 86, 83]. Several experimental satellite SARs such as SEASAT [92] and SIR-B [31] demonstrated the usefulness of SAR. Canada Center for Remote Sensing (CCRS) launched RADARSAT on November 4, 1995, a satellite SAR intended for civilian Earth observation applications.

2.5.2 Speckle noise in SAR images

SAR generates images by coherent processing of returned radar signals and hence, the SAR images are subject to speckle effects. Figure 2.14 shows a representative SAR



Figure 2.14: A typical SAR amplitude image

(A typical SAR amplitude image in which the speckle patterns are evident. Used with permission of the Canada Center for Remote Sensing (CCRS), Canada).

image calculated from a flight by airborne SAR over a region near Ottawa, Canada. The images in the data set include mixed terrain, farm land, industrial and frozen river regions. It can be observed from this image that the speckle is significant in mixed terrain and industrial (high intensity homogeneous) regions when compared to the frozen river (low intensity homogeneous) regions as is characteristics of speckle. Such images may require filtering operations such as speckle reducing filters [23, 47, 52, 90] or edge detection algorithms designed for the particular interfering noise [3, 24, 82] environments in order to achieve good performance in image processing applications.

2.5.3 SAR image data processing

Images obtained using SAR can be grouped into different types based on data processing techniques used in image formation. First, SAR images can be classified based on the radar return signal component used in computing the response at a single pixel (i.e. resolution element) in the recorded image. These are:

- Amplitude SAR images
- Intensity SAR images
- **Amplitude SAR image**

In theory, the received radar signal at an observation point consists of sums of delayed and attenuated copies of the transmitted signal. It was mentioned in Section 2.2.1 that coherent processing retains phase information, thus the received signal consists of in phase and quadrature components. The sum of complex signals results in another complex quantity and is referred as complex amplitude speckle signal. Derin [15] derived the probability density function of the real complex amplitude SAR image expressed as:

$$p(A) = A \frac{\exp(-A^2/2\sigma^2)}{\sigma^2}, \quad A \geq 0 \quad (2.24)$$

where x and y are the in-phase and quadrature components of the SAR signals and $A = \sqrt{x^2 + y^2}$.

Derin derived the amplitude SAR image mean calculated over homogeneous regions which is found to be $\mu_A = \sigma\sqrt{\pi/2}$ and the variance $\sigma_A^2 = 2 - \pi/2\sigma^2$ where σ is the standard deviation of the normally distributed in-phase x and quadrature y components. The amplitude SAR image therefore exhibits a ratio of standard deviation to mean of $\sigma_A/\mu_A = 0.5227$ over homogeneous regions [15].

- **Intensity SAR image**

SAR intensity images are formed by computing the sum of the in phase x and quadrature y components yielding SAR intensity image resolution element equal to $I = x^2 + y^2$. Derin [15] also derived the probability density function of the intensity SAR image expressed as:

$$p(I) = \frac{1}{2\sigma^2} \exp(-I/2\sigma^2), \quad I \geq 0 \quad (2.25)$$

having mean $\mu_I = 2\sigma^2$ and variance of $\sigma_I^2 = 4\sigma^4$ where σ is the standard deviation of the normally distributed in-phase x and quadrature y components. Thus an intensity SAR image is characterized by its ratio of the standard deviation to mean over homogeneous regions equal to unity [15].

Secondly, another way of classifying SAR images is based on the number of looks considered in image formation. These images are classified into:

- Single Look or One-Look SAR
- Multilook SAR image
- **Single-look and Multilook SAR**

Single-look or one-look SAR images are obtained by considering a single realization

of intensity or amplitude SAR images. Multilook SAR images are obtained by combining realizations from several single-look images to form composite response. If N single-look SAR images are averaged on an intensity basis then the resulting SAR image is called an N -look intensity SAR image.

The probability density function of single-look amplitude and intensity images is expressed by Equations 2.24 and 2.25, respectively. The probability density function of 4 - look amplitude SAR image denoted by A found to be χ distributed [15] and is expressed as:

$$p_4(A) = 16A^7 \exp(-A^2/\sigma^2)/3\sigma^8, \quad A \geq 0 \quad (2.26)$$

where σ equal to the standard deviation of the normally distributed in-phase x and quadrature y radar return signal components. The ratio of the standard deviation to mean over homogeneous regions is therefore $\sigma_4(A)/M_4(A) = 0.2536$ for 4 - look amplitude SAR images.

Derin [15] also derived the corresponding probability density function for 4 - look intensity I , is χ^2 distributed and is expressed as:

$$p_4(I) = 8I^3 \exp(-2I/\sigma_2)/3\sigma^8, \quad I \geq 0 \quad (2.27)$$

where σ is the standard deviation of the normally distributed in-phase x and quadrature y components of the radar return signal. The ratio of the standard deviation to mean over homogeneous regions is found to be equal to $\sigma_4(I)/\mu_4(I) = 0.5$. For single-look intensity SAR images mean and standard deviation over homogeneous regions are equal whereas for multi-look (N - look) amplitude SAR images these quantities are proportional.

In order to reduce the undesirable effects of speckle noise, several independent (single-look) SAR images can be averaged thus producing a multi-look SAR image. While the multi-look process reduces the speckle noise, it will also reduce image resolution due

to spatial averaging. However, multi-look images are often better suited to applications. For example, Lee [55] suggested that multi-look SAR images are better suited to image segmentation and classification applications despite their reduction in azimuth resolution.

2.5.4 Speckle noise models

Image noise models are of particular importance for digital processing of images. In this section, models of speckled images are considered with particular reference to radar images. Several researchers have proposed models for SAR speckled images as a prelude to the development of different algorithms for SAR images. A brief review of these algorithms is presented in this section.

Lee proposed that a multiplicative noise model can be used for simulating SAR image speckle [57] as.

$$y(i, j) = x(i, j) \cdot n(i, j) \quad (2.28)$$

where, $y(i, j)$ is the recorded SAR image, $x(i, j)$ is the original noise-free signal and $n(i, j)$ is the interfering random noise field. The noise signal $n(i, j)$ is Rayleigh distributed with mean of one and standard deviation equal to $[\frac{1}{\pi} - 1]^{1/2} = 0.522$. With the use of multiplicative noise model represented by Equation 2.28 speckle corruption is a point operation and hence $y(i, j)$ is uncorrelated whenever $x(i, j)$ is uncorrelated. Durand *et al.* used multiplicative noise model similar to Lee for simulating SAR speckle which they used for SAR data filtering and classification [17]. Kuan *et al.* suggested a non-stationary mean and non-stationary variance (NMNV) model for use in image restoration algorithms for speckled images [51].

Tur *et al.* noted that a simple multiplicative noise model may not be a good choice

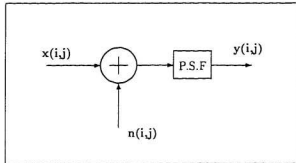


Figure 2.15: Speckle noise model

for modeling speckle noise as it fails to account for inter-pixel correlation effects due to correlation in speckle itself. Frost *et. al* [23] used a multiplicative-convolutional speckle image model to eliminate fading effect (dominant source of randomness in radar images) and hence derived minimum mean squared error (MMSE) estimates for use in SAR data filtering. Frost *et. al.* suggested that SAR images be modeled as,

$$y(i, j) = [x(i, j) \cdot n(i, j)] \star h(i, j) \quad (2.29)$$

where \star indicates convolution with the SAR impulse response $h(i, j)$.

Based on their model for speckled noise, Frost *et. al.* also developed an edge detection algorithm for SAR images [24]. Hudson and Jernigan [47] used a multiplicatively convolved model similar to Frost but with a circularly Gaussian point spread function (*PSF*) impulse response. Figure 2.15 shows a speckle noise model used by Frost *et. al.* Zaman and Moloney [90] used models of single-look and 4-look amplitude images suggested by the Hudson *et. al.* [47] to generate simulated SAR speckle on which to test edge preserving noise-smoothing quadratic volterra filters.

More complex models for simulating speckle noise have also been proposed such as Derin [15, 52] which are based on radar signal model. However, the model suggested by Frost *et. al.* have been found to be adequate for explaining the speckle noise observed in images formed by coherent imaging systems [24, 47, 89]. Frost *et. al.* noted that the above multiplicative-convolved speckle image model also explains SAR image adequately so that the speckled statistical properties images simulated according to Equation 2.29 are comparable to that of actual SAR imagery.

2.6 Summary

This chapter began with a review of the literature on speckle noise in images. A review of speckle noise nature and characteristics were outlined. A survey into edge detection methods in general and methods that are suited to use on speckled images was conducted. Algorithms for speckle specific edge detection available in literature were briefly introduced. The advantages and disadvantages of several speckle specific edge detection methods were reviewed. Background information on imaging technology used in SAR imaging systems was provided. SAR data processing methods and types of SAR images along with their statistical models were outlined. Speckle image noise models available in the literature were reviewed and a radar signal noise model is introduced. The literature search into edge detection methods reveals that ratio based methods are better suited for use on speckled images. Hence methods that use ratios between pixel values are considered for further investigation and analysis. An evaluation of edge detection methods for speckled images using synthetic and real airborne SAR images is presented in the next Chapter.

Chapter 3

Evaluation of Edge Detection Methods for Speckled Images

3.1 Introduction

In this chapter, the procedure previously used by Zaman and Moloney [90, 91] to measure the performance of edge detection methods for speckled images is reviewed. Since the previous evaluations by Zaman and Moloney [91] mainly used synthetic data, a study of these methods using real airborne SAR images with permission from Canada Center for Remote Sensing is conducted. An evaluation of existing edge detection methods using real images with real speckle is performed in this Chapter.

3.2 Edge detector performance measures

Since all edge detectors are not suitable for all applications, the performance of a given edge detector must be carefully evaluated before selecting it for a particular application. Moreover, at times the use of a particular edge detector may be computa-

tionally inefficient as the same results may be obtained using a computationally simpler edge detector. Edge detector performance measures are also important as they may aid in designing new operators by providing guidelines on how to improve the existing edge detection operators. In this section measures used in evaluating edge detector performances in this thesis are presented.

The evaluation of an edge detector's performance is usually conducted based on both *qualitative* and *quantitative* factors and this practice is followed in this thesis. Qualitative evaluations are conducted mainly based on human perception. Quantitative evaluations are based on several appropriate edge detector quantitative performance measures. Other evaluation methods used in computer vision applications which are supported by knowledge base systems, artificial intelligence decision rules, fuzzy logic etc., are not addressed.

3.2.1 Qualitative performance measures

Evaluation of an edge detector's output can yield quick and obvious insights into the performance of an edge detector. An edge map obtained using an edge detection operator is visually compared with an ideal edge map obtained for the noise-free image in order to determine whether or not a close match exists between the two edge maps. In case of real test data for which the ideal edge map is not available, qualitative evaluation is performed by comparing the detected edge map with a human perceived edge map. Such qualitative inspection aids in evaluating an edge detector's performance by providing rapid answers to questions such as:

- Does the edge map contain any spurious (false) edges ?
- Does the edge map give a close estimate to the ideal edge map ?

- Does the edge map give a close estimate to the human perceived edge map ?
- Is the edge map missing any true edge information ?

Qualitative inspection can act as a preliminary examination tool in the case of synthetic test data for which final evaluation decisions can be mainly based on quantitative evaluation measures. However, the qualitative evaluation plays an important role in the evaluation of an edge detection operator's performance on real data such as SAR for which the information regarding the ideal conditions may not be available.

3.2.2 Quantitative performance measures

Pratt [77] suggests that a single figure of merit be used to measure edge displacement, ambiguity and incorrect classification etc. :

$$R = \frac{1}{\max(N_A, N_I)} \frac{1}{1 + \beta d^2}, \quad (3.1)$$

where N_A and N_I are the total number of edge pixels in the actual and ideal edge maps, respectively. The parameter d is the perpendicular distance from an actual edge pixel to ideal edge pixel and β is a scaling constant.

McLean and Jernigan [66] suggested that edge detector performance be measured in terms of edge pixel correctness, ambiguity, displacement and missed edge pixels, which can be expressed using four different parameter values. Based on their work Zaman and Moloney [90] suggested a new set of measures for evaluating edge detector performance. The measures are named *correct*, *ambiguous*, *missed* and *wrong*. These factors are defined as:

$$C = \frac{2 \times (\#correct)}{(\#true + (\#found))} \quad (3.2)$$

$$A = \frac{\#ambiguous}{\#true} \quad (3.3)$$

$$M = \frac{\#missed}{\#true} \quad (3.4)$$

$$W = \frac{\#false}{\#found} \quad (3.5)$$

- *#true* : total number of edge pixels in the ideal edge map.
- *#found* : number of edge pixels found in the detected edge map being evaluated.
- *#correct* : number of true edge pixels found with either one or two detected edge pixels within a 5x5 window centered on the true edge pixel location.
- *#ambiguous* : number of true edge pixels found with more than one detected edge pixel a 5x5 window centered on the true edge pixel location.
- *#missed* : number of true edge pixels found with at least a single detected edge pixel within a 5x5 window centered on the true edge pixel location.
- *#wrong* : number of detected edge pixels not found within a 5x5 window of any true edge pixel location.

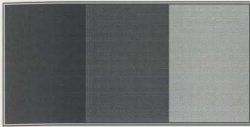
Pratt's figure of merit, R gives a single value for an edge detectors performance which may not be sufficient to completely describe the various facts of the operator's performance. This figure of merit tends to favor a small number of detected edges, even if there are large gaps between detected pixels [66]. Moreover, such a single-valued measure may highlight only limited aspects of an edge detection operators performance. Different aspects of an operator's performance should be examined in order to know how well the algorithm performs and to know the deficits of that particular algorithm etc. The measures suggested by Zaman and Moloney have been found to be most appropriate in the quantitative evaluation of edge detector performance [90] and are used in this thesis.

3.3 Speckle noise simulation

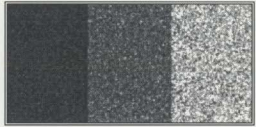
Reviewed speckle noise models in Section 2.5.4, show that multiplicative-convolved model suggested by Frost *et. al.* is adequate to simulate SAR speckle imagery. Accordingly, the multiplicatively convolved spatially correlated speckle noise model shown in Figure 2.15 and Equation 2.29, previously used by Frost [23, 24], Hudson [47] and Zaman [89], are used for simulating speckle images in this thesis.

The procedure used by Zaman [89] to generate speckle image according to Equation 2.29 is briefly outlined here. A 2-D noise field of the image size to be corrupted with each pixel value drawn for a χ^2 distribution, with 8-degrees of freedom is obtained. Each image pixel in the original noise-free image is multiplied point-wise with samples from the noise model file. The resulting multiplicative model of the image is then convolved with a circularly Gaussian PSF to obtain a 4 - *look* amplitude SAR image model.

The validity of the simulated speckle noise model is tested using two sample images *Spectrum* and *Ramp*. The original test image *Spectrum* consists of three regions with constant intensities 40, 80 and 160, respectively. The second test image *Ramp* consists of three regions with left most and right most regions of constant intensities 40 and 160 respectively and a middle regions of a gradually increasing intensity in X-direction ranging from 40 to 160. The original sample test images *Spectrum* and *Ramp* are then corrupted by the previously described speckle simulation process. From Figure 3.1 it can be seen that the simulated speckle is multiplicatively signal-dependent in nature. i.e speckle noise is more significant in high intensity homogeneous regions than in low intensity homogeneous regions. For example, in the corrupted *Ramp* test image it can be seen that the speckle noise is less prominent in low intensity region (left) and more significant in the high intensity homogeneous regions (right) with a gradual change in



(a)



(b)



(c)



(d)

Figure 3.1: Generation of synthetic speckle image

(a) Original *Spectrum* ; (b) Simulated speckled *Spectrum*

(c) Original *Ramp* ; (d) Simulated speckled *Ramp* .

Estimates of the standard deviation to mean ratio on the simulated speckled *Spectrum* image.

Sample region Intensity I	Mean μ	Std. σ	Rho $\rho = \sigma/\mu$
$I= 40$	37.38	9.70	0.2597
$I= 40$	40.14	9.18	0.2287
$I= 80$	101.72	25.74	0.2530
$I= 80$	96.50	23.90	0.2476
$I= 80$	92.72	21.91	0.2363
$I= 160$	195.52	39.95	0.2043

Table 3.1: Standard ratio test for simulated speckle noise.

speckle prominence in the middle region.

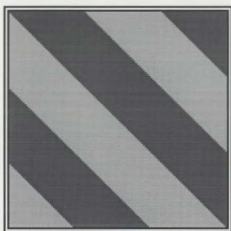
Table 3.1 shows speckle signal to noise ratio (*SNR*) ρ value calculated for image samples collected from the simulated speckled image *Spectrum* Figure 3.1(b). Several 16×16 pixel image samples are extracted from different homogeneous intensity regions of Figure 3.1(b). Standard deviation (σ) and mean (μ) values are calculated for the extracted image samples. As a standard measure of practice, the ratio of standard deviation (σ) to mean (μ) is calculated indicating the speckle *SNR Rho* ($\rho = \sigma/\mu$) value [23, 55]. Test results from Table 3.1 show that the ratio ρ is almost constant (equal to 0.2383), confirming speckle characteristics for simulated speckle image [23, 55].

3.4 Test data

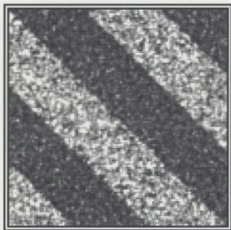
Test images for evaluating edge detector performance include both synthetic and real airborne SAR images of varying scene contents, structures and business. The term structures used to refer to image objects or patterns in terms of their length and width as measured in units of single resolution elements or pixels. If input image consists of an object 30×40 pixels it may be referred to as a large structure if image also consist of an object 3×5 pixels which is then referred to as small structure. The term business is used to refer how closely positioned or how repetitive the image structures are in the underlying image. These definitions are only mandatory and may not be the standard definitions for "structure" or "busyness".

3.4.1 Synthetic speckled images

The performance of existing edge detection methods has been evaluated on test images similar to those of Figure 3.1 which have been corrupted according to the process described in Section 3.3. The original images used for synthetic test images include both computer generated patterns and photographic images of outdoor scenes. The computer generated test images include the images *Spectrum*, *Ring* and *Strips*. The *Spectrum* original and speckled images are shown in Figure 3.1(a) and (b). The *Strips* and *Ring* original and speckled images are shown in Figure 3.2(a), (b) and Figure 3.3(a), (b) respectively. Test images *Strips* and *Ring* consist of two regions of gray scale intensities 100 and 200 indicating dark and bright regions respectively. The test image *Combine* consists of an outdoor scene image *Balloon*, combined with the test images *Strips* and *Ring* and allows testing using outdoor scene detail.



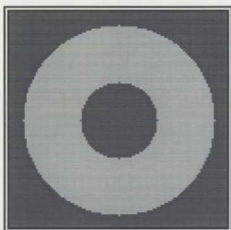
(a)



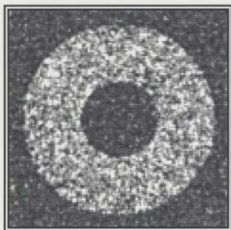
(b)

Figure 3.2: Synthetic test image *Strips* :

(a) Original *Strips* ; (b) Simulated speckled image based on (a).



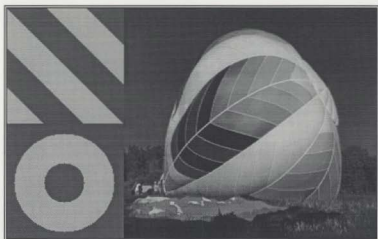
(a)



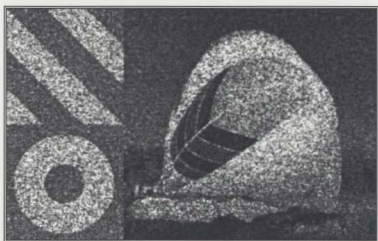
(b)

Figure 3.3: Synthetic test image *Ring* :

(a) Original *Ring* ; (b) Simulated speckled image based on (a).



(a)



(b)

Figure 3.4: Synthetic test image *Combine* :

(a) Original *Combine* ; (b) Simulated speckled image based on (a).

3.4.2 Real airborne SAR images

Several real airborne SAR images obtained from Canada Center for Remote Sensing (CCRS), Ottawa are also used as test data containing real speckle noise. The SAR test images denoted as *Moderately Busy*, *Busy*, *Fields*, *Highway*, *Industrial* and *Smooth* are selected for testing and evaluation. These images represent a variety of scene contents. The SAR test images *Moderately Busy*, *Busy* and *Smooth* are introduced and used in this Chapter. The other SAR test images *Fields*, *Highway* and *Industrial* are introduced and used later in this thesis. Evaluation of previous speckle-specific edge detection methods for SAR images was conducted using SAR test images *Moderately Busy*, *Busy* and *Smooth*.

The test image *Moderately Busy* shown in Figure 3.5 consists of woods, fields and roads and represents images which consist of several low and high contrast regions and definite edge information. Test image *Busy* shown in Figure 3.6 contains predominantly fine structures and is “busy” as a consequence. The underlying image is a suburban city area, which has several straight roads and rows of houses in the ordered manner of man-made structures. The test image *Smooth* shown in the Figure 3.7 consists of an area of a frozen river and hence has only a few low contrast details such as cracks in the ice etc.

Standard ratio tests were applied to the SAR images of Figures 3.5, Figure 3.6 and Figure 3.7 over homogeneous regions. Small regions of size 8×8 were extracted yielding an estimate of the standard deviation to mean ratio of approximately 0.3238 which is found to be close to the theoretical values [23] thus confirming these SAR images exhibit speckle characteristics [54, 55].

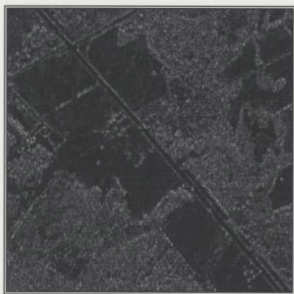


Figure 3.5: Real airborne SAR test image *Moderately Busy* .



Figure 3.6: Real airborne SAR test image *Busy* .

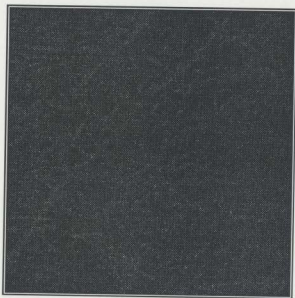


Figure 3.7: Real airborne SAR test image *Smooth* .

3.5 Evaluation of edge detection methods

3.5.1 Evaluation using synthetic test images

The synthetic test images *Strips*, *Ring* and *Combine* are used to evaluate the performance of existing edge detectors performance. Ideal edge maps for these images are obtained by applying the Sobel operation of Equation 2.6 to the respective noise-free images. Existing speckle-specific edge detection methods are used to generate edge maps for the corresponding simulated speckled images. These evaluations are similar to the methods used by Zaman and Moloney [90], however tests conducted here are mainly to give insight into the existing speckle-specific edge detection operators.

Figure 3.8(a) shows the edge map for the *Strips* image obtained on the noise-free image of Figure 3.2(a) using Sobel operator of Equation 2.6. Figure 3.8(b) shows the Coefficient of Variation (CoV) edge map for the speckled *Strips* of Figure 3.2(b) obtained using Equation 2.9 with mask size $N = 5$ and threshold $T = 0.29$. Figures 3.8(c) to (f) shows edge maps for speckled *Strips* obtained using Bovik RoA (Section 2.4.2), Touzi CFAR (Section 2.4.3), MRoA (Section 2.4.4) and RGoA (Section 2.4.5) edge detectors respectively, with mask size $N = 7$ and threshold values as shown in Table 3.2. The mask size (s) and threshold values used here are selected after conducting several experiments and represent the most promising values for each of the selected edge detector for the images under test. Figures 3.8(g) and (h) represent the edge maps obtained using the MRoA and RGoA method followed by edge thinning recommended for the MRoA and RGoA methods [89].

Similar tests conducted for the *Ring* (Figure 3.3) test images and corresponding edge maps obtained using the parameters listed in Table 3.2 for different edge operators are shown in Figure 3.9. The test results for the *Combine* images are shown in Figures 3.10

and cited in the Table 3.3.

Qualitative analysis: Evaluations of edge detector performance by qualitative inspection based on human perception confirm that the MRoA and RGoA methods are better relative to the other previous speckle specific edge detection methods. The methods generate edge maps with better suppression of spurious edge pixel information in non-edge regions. Their edge maps are found to be better in giving better definition to boundaries between regions. However, several true edge pixels in the corresponding ideal edge maps are missing in the MRoA and RGoA edge maps for the speckled images. These two methods also generated thick edge maps leading to a requirement for edge thinning post-processing operations in order to produce thin and more precise edge maps. Qualitative analysis test results obtained here confirm previous evaluation test results obtained by Zaman and Moloney [91].

Quantitative analysis: The evaluation of the edge detection method's performance using the quantitative measures suggested by Zaman and Moloney [89] also found that the MRoA and RGoA methods generated meaningful edge maps when compared to the other methods. The methods resulted high C values indicating edge maps with improved number of correct edge pixels detected. The measures for W , M and A are also found to be relatively better (i.e. low values) when compared with the test results of the other edge detectors cited in Table 3.2 and Table 3.3 indicating less number of wrong edge pixels detected with low missing and ambiguous edge pixel measures. Quantitative evaluation of edge detection methods conducted here confirm test results obtained by Zaman and Moloney [90] using synthetic test images.

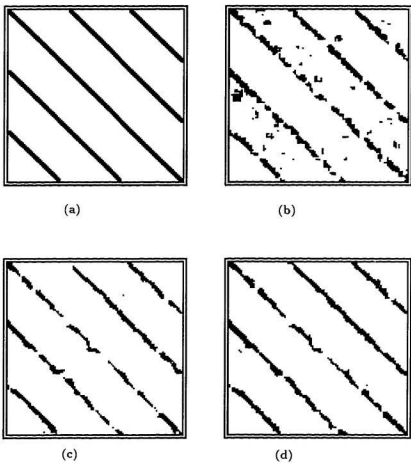
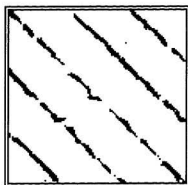
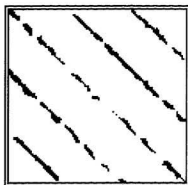


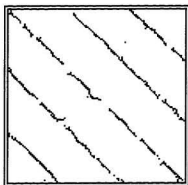
Figure 3.8: Edge maps obtained for the *Strips* images:
(a) Sobel edge map for Figure 3.2(a); (b) CoV edge map for Figure 3.2(b);
(c) RoA edge map for Figure 3.2(b); (d) Touzi edge map for Figure 3.2(b).



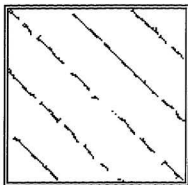
(e)



(f)



(g)



(h)

Figure 3.8: Edge maps obtained for *Strips* images:

(e) MRoA edge map for Figure 3.2(b); (f) RGoA edge map for Figure 3.2(b);

(g) Edge thinning on Figure 3.8(e); (h) Edge thinning on Figure 3.8(f).

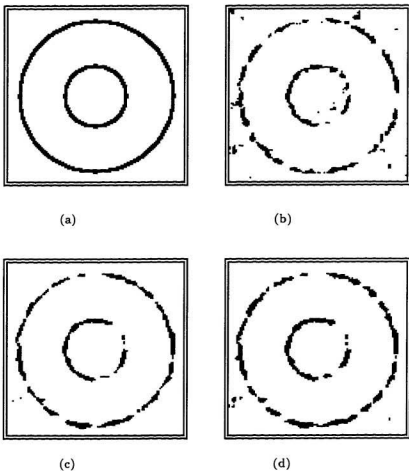
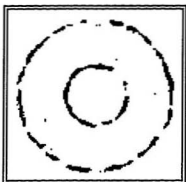
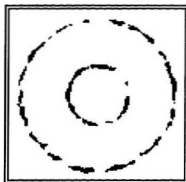


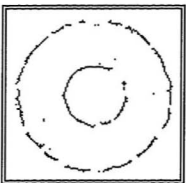
Figure 3.9: Edge maps obtained for *Ring* images:
(a) Sobel edge map for Figure 3.3(a); (b) CoV edge map for Figure 3.3(b);
(c) RoA edge map for Figure 3.3(b); (d) Touzi edge map for Figure 3.3(b).



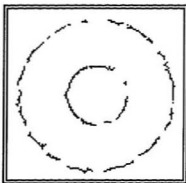
(e)



(f)



(g)



(h)

Figure 3.9: Edge maps obtained for *Ring* images:

- (e) MRoA edge map for Figure 3.3(b); (f) RGoA edge map for Figure 3.3(b);
(g) Edge thinning on Figure 3.9(e); (h) Edge thinning on Figure 3.9(f).

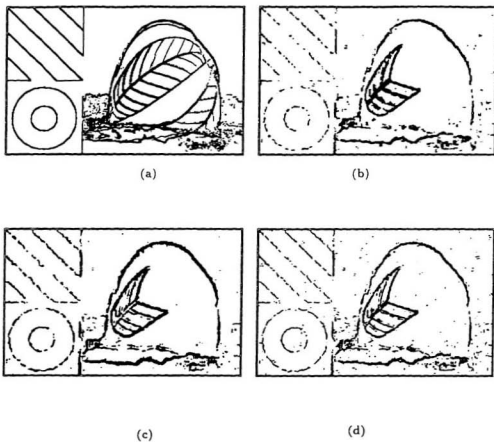
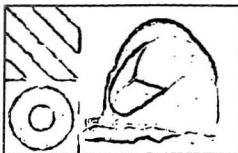
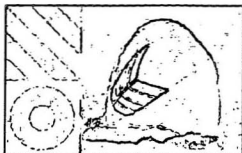


Figure 3.10: Edge maps obtained for *Combine* images:

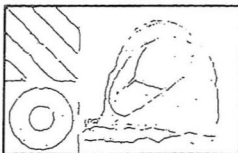
- (a) Sobel edge map for Figure 3.4(a); (b) Coeff. edge map for Figure 3.4(b);
 (c) RoA edge map for Figure 3.4(b); (d) Touzi edge map for Figure 3.4(b).



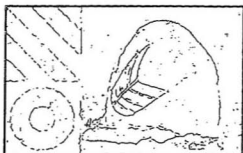
(e)



(f)



(g)



(h)

Figure 3.10: Edge maps obtained for *Combine* images:

(e) MROA edge map for Figure 3.4(b); (f) RGoA edge map for Figure 3.4(b);

(g) Edge thinning on Figure 3.10(e); (h) Edge thinning on Figure 3.10(f).

Test Image	Edge Detector	Figure	Mask N	Threshold		C in %	M in %	W in %	A in %
				T_g	T_r				
Test Image Strips :									
Original	Sobel	3.2(c)	-	20	-	100.00	0.00	0.00	0.00
Speckled	Sobel	3.2(d)	-	240	-	22.38	0.68	69.53	47.78
..	CoV	3.2(e)	5	-	0.29	57.62	5.88	14.91	35.47
..	Touzi	3.2(f)	7	-	0.63	70.50	2.67	1.49	29.51
..	RoA	3.2(g)	7	-	1.95	52.39	9.02	2.77	39.52
..	MROA	3.2(h)	7	-	0.61	87.75	6.11	1.39	16.36
..	RGoA	3.2(i)	7	85	0.58	88.96	13.07	0.12	14.22
Test Image Ring :									
Original	Sobel	3.3(c)	-	20	-	100.00	0.00	0.00	0.00
Speckled	Sobel	3.3(d)	-	140	-	12.42	0.08	76.25	59.66
..	CoV	3.3(e)	5	-	0.32	63.69	14.89	9.31	28.10
..	Touzi	3.3(f)	7	-	0.59	74.45	9.04	2.60	24.55
..	RoA	3.3(g)	7	-	2.0	59.44	10.28	4.33	33.24
..	MROA	3.3(h)	7	-	0.58	85.32	13.74	0.27	16.13
..	RGoA	3.3(i)	7	85	0.56	82.04	16.40	0.72	17.37

Table 3.2: Quantitative performance measures on synthetic test images

$$C = \frac{2x\#correct}{\#true + \#found}$$

$$W = \frac{\#wrong}{\#true}$$

$$M = \frac{\#miss}{\#true}$$

$$A = \frac{\#ambig}{\#true}$$

Test Image	Edge Detector	Figure	Mask N	Threshold		#found	C in %	M in %	W in %	A in %
				T_g	T_r					
Test Image Combine										
Original	Sobel	3.10(a)	3	100	—	13184	100.00	0.00	0.00	0.00
Speckled	CoV	3.10(b)	5	-	0.35	7746	49.50	39.29	4.71	21.40
..	Touzi	3.10(d)	5	-	0.58	7587	63.00	32.89	5.48	17.47
..	RoA	3.10(c)	7	-	2.0	9974	43.86	41.39	5.75	23.09
..	MRoA	3.10(e)	5	-	0.55	6506	63.16	47.70	11.66	7.95
..	RGoA	3.10(f)	5	83	0.55	6827	62.73	43.80	4.21	11.53

Table 3.3: Quantitative performance measures on synthetic test images

$$C = \frac{2 \times \#correct}{\#true + \#found}$$

$$W = \frac{\#wrong}{\#true}$$

$$M = \frac{\#miss}{\#true}$$

$$A = \frac{\#ambig}{\#true}$$

3.6 Evaluation of edge detection methods for real airborne SAR images

Edge detector evaluation using real airborne SAR data set is based on the three images *Moderately Busy*, *Busy* and *Smooth*. Edge maps were obtained for all three images using the MRoA and RGoA edge detection methods only. These edge detection operators were selected for further evaluating, since, test results illustrated in Figures 3.8, 3.9, 3.10 confirmed that these operators perform better than the other existing edge detectors.

Figure 3.11(b) shows the MRoA edge map for the *Moderately Busy* test image obtained using mask size $N = 7$ and ratio threshold $T_r = 0.475$. The RGoA edge map for this image is obtained using mask size $N = 7$, ratio-threshold $T_r = 0.475$ and gradient threshold value $T_g = 50$, and is shown in Figure 3.11(c). Figures 3.12(b) and (c) show the corresponding edge maps on the *Busy* test image using the same parameters used for the *Moderately Busy* test image.

The MSPRoA edge map on *Smooth* image is obtained using mask size $N = 7$, ratio-threshold $T_r = 0.525$. RGoA edge map for this SAR test image is obtained using $N = 7$, $T_r = 0.525$ and $T_g = 65$. Test results for the *Smooth* test image are shown in Figures 3.13 (b) and (c). The RGoA edge maps are followed by edge thinning post-processing operations recommended to use on this method by Zaman and Moloney [90]. The corresponding edge RGoA edge thinning edge maps for *Moderately Busy*, *Busy* and *Smooth* test images are shown in Figure 3.5(d), Figure 3.6(d) and Figure 3.7(d) respectively.

- **Qualitative analysis**

Since the test cases consist of real airborne SAR images, ideal edge maps are not

available for comparison. However, from figures 3.11, 3.13, 3.12 it can be seen that both the MRoA and RGoA methods are successful in extracting accurate edge information from the real airborne SAR test images.

Small regions of size 16×16 pixels extracted over edge regions in the *Moderately Busy* and *Busy* test images as shown in Figure 3.14. The MRoA and RGoA edge maps on these images are obtained and are also shown in Figures 3.14. These test results show that the RGoA method extracted some edge pixels that are missing in the MRoA edge maps. The better performance of the RGoA method may be attributed to the gradient edge strength information included into this operator.

However, visual inspection of the edge maps for SAR test images *Moderately Busy*, *Busy* and *Smooth* or extracted samples images on these images show that the MRoA and RGoA operators are not successful in extracting all true edges information from these images. The edge map for *Moderately Busy* SAR image found to be missing several edge pixel information compared to the human perceived edge map for this image. Where as, test results on SAR *Busy* show that extracted edge map for this image consist of several false edge pixel information compared to human perceived edge map for this image.

Both methods performed poorly on SAR test image *Smooth*, partly due to the lack of contrast in this image. As with the synthetic test images, the edge detectors also resulted in thick edge maps for the real airborne SAR images.

Quantitative analysis

A form of quantitative performance measure for the real SAR test images was obtained by extracting small sample regions from homogeneous regions and edge areas. An edge detection operator is expected to detect zero edges over homogeneous regions. Small areas of size 8×8 samples were extracted from both high intensity and low intensity homogeneous regions of *Moderately Busy* and *Busy* test images. In addition similar

Region of Interest	# Edge Pixels		Mean	Std	$\rho =$ Std/Mean
	RGOA	MROA			
MB, Dark	2	1	22.1279	5.7003	0.2576
MB, Bright	0	0	63.7383	19.3530	0.3036
MB, Edge	56	47	56.2998	27.2472	0.4840
B. Dark	0	0	15.2304	4.3115	0.2831
B. Bright	1	3	60.1289	24.0287	0.3996
B. Edge	28	37	56.6367	37.6114	0.6641

Table 3.4: Evaluation of edge detection methods for real airborne SAR images

test samples from edge areas were extracted from these images. The number of edge pixels detected for these test samples by the MROA and RGOA methods were calculated. The test results showing performance of these edge detectors are shown in Table 3.4.

These methods performed satisfactorily on SAR images but did miss some edge pixels that can be detected by the human vision systems. In addition edge maps resulted in multiple responses to single edge resulting in thick edge maps.

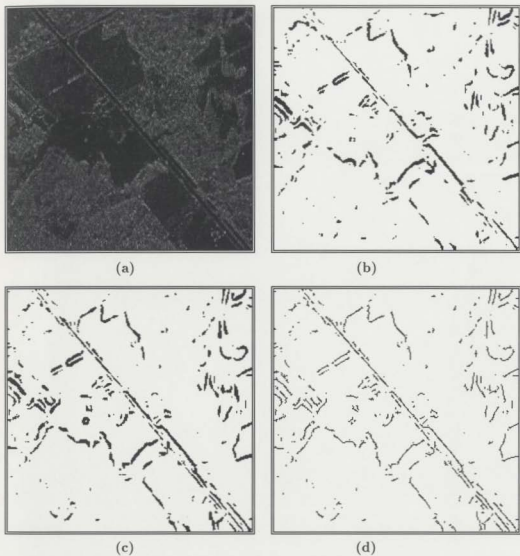


Figure 3.11: Edge maps for SAR image *Moderately Busy* :

- (a) SAR *Moderately Busy* ; (b) MRoA edge map for (a) [$N = 7, T_r = 0.475$]; (c) RGoA edge map for (a) [$N = 7, T_r = 0.475, T_s = 50$]; (d) Edge thinning on (c).

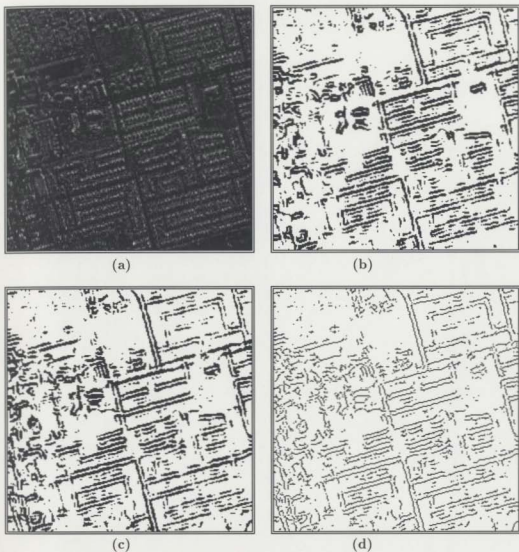


Figure 3.12: Edge maps for SAR image *Busy* :

- (a) SAR test image *Busy* ; (b) MRoA edge map for (a) [$N = 7$, $T_r = 0.475$]; (c) RGoA edge map for (a) [$N = 7$, $T_r = 0.475$, $T_g = 50$]; (d) Edge thinning on (c).

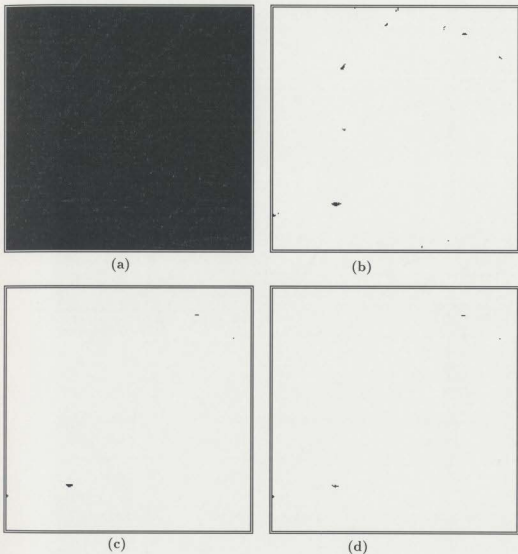


Figure 3.13: Edge maps for SAR image *Smooth* :

- (a) SAR test image *Smooth* ; (b) MRoA edge map for (a) [$N = 11, T_r = 0.6$]; (c) RGoA edge map for (a) [$N = 11, T_r = 0.6, T_g = 50$]; (d) Edge thinning on (c).



(aa)



(ab)



(ac)



(ba)



(bb)



(bc)



(ca)



(cb)



(cc)

Figure 3.14: Evaluation of edge detection methods for 16×16 SAR test samples:

(aa) Test sample #1 ; (ab) Test sample #2 ; (ac) Test sample #3 ;

(ba) MRoA on (aa) ; (bb) MRoA on (ab) ; (bc) MRoA on (ac) ;

(ca) RGoA on (aa) ; (cb) RGoA on (ab) ; (cc) RGoA on (ac) ;

Chapter 4

Maximum Strength Edge Pruned Ratio of Averages Edge Detector

4.1 Introduction

In this chapter a ratio edge detector for speckled images based on maximum strength edge pruning (MSPRoA) is developed which considers explicitly both edge magnitude strength and orientation information. The proposed edge detection method is different from previous ratio-based methods in that it makes a more explicit use of edge orientation information that is implicitly expressed in other ratio based methods. This additional information is found to be helpful in confirming true edge pixels by the MSPRoA edge detection operator. The MSPRoA algorithm is presented in this chapter, along with worked examples based on 1-D graphical illustrations and simple computer generated images.

4.2 The MSPRoA edge detection method

4.2.1 Terminology

This section defines various terms necessary to characterize and explain the MSPRoA algorithm. Figure 4.1 illustrates a graphical view of some of these terms.

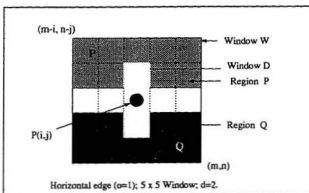


Figure 4.1: A general pattern computing MSPRoA strength, $N = 5$, $d = 2$.

- The MSPRoA edge strength measure $R(r, o)$: The edge strength value measured using the MSPRoA method is expressed as a vector quantity $R(r, o)$ having both magnitude $R(r)$ and direction $R(o)$.
- The pruning (or correlation) distance parameter d : The pruning (or correlation) distance parameter d is used in pruning candidate edge pixels based on maximum edge strength values to obtain true edge pixels. This parameter is used in deciding which edge pixels are to be selected into a sub-window D (defined later in this section).

- The sub-window D : If d is the pruning distance parameter the sub-window D consists of $(2d - 1)$ pixels arranged as a one-dimensional array centered about the $P(i, j)$ pixel of interest, with orientation perpendicular to the direction $R(o)$ of a potential edge candidate at position $P(i, j)$.
- The maximum edge strength measure $D(r)$: The pruning edge strength magnitude $D(r)$ is the minimum $R(r)$ (the maximum edge strength) value of all the pixels selected by a D sub-window.

4.2.2 The MSPRoA algorithm

Consider a given processing window W pixels of mask size N centered on image pixel of interest $P(i, j)$. For each of the selected edge orientations as shown in Figure 4.2, image pixels within this processing window are assigned as appropriate, to one of two non-overlapping regions P and Q . The MSPRoA method uses the following sequence of steps to classify $P(i, j)$ as either an edge or a non-edge pixel:

- For each image pixel $P(i, j)$ the ratio of averages edge strength magnitude is calculated using the MRoA method as reviewed in Section 2.4.4. This value is recorded as the MSPRoA edge strength magnitude $R(r)$ of the pixel $P(i, j)$.
- The direction in which the minimum MRoA edge strength $R(r)$ value is found is recorded as the MSPRoA edge orientation $R(o)$ of the pixel $P(i, j)$.
- The pixel $P(i, j)$ is selected as a *candidate* edge pixel if:

$$R(r) < T_r \quad \text{where } T_r \text{ is a user selected ratio-threshold.} \quad (4.1)$$

- If $P(i, j)$ is a *candidate* edge pixel then edge pixels neighboring $P(i, j)$ within a D sub-window as shown in the Figure 4.2 are examined. The minimum $R(r)$ value of

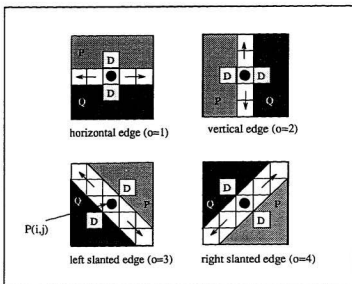


Figure 4.2: Schematic of the MSPRoA edge detector.

all the pixels within sub-window D is calculated and is assigned as the maximum edge strength measure $D(r)$ of the *candidate* edge pixel $P(i, j)$.

- A *candidate* pixel $P(i, j)$ is selected as an *edge* pixel if:

$$R(r) = D(r) \quad (4.2)$$

Otherwise *candidate* pixel $P(i, j)$ is rejected as an edge pixel.

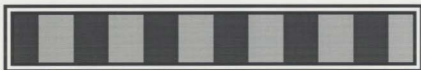
- All other non-candidate image pixels are labeled as non-edge pixels.

4.2.3 Graphical illustration using 1-D signals

The operation of the MSPRoA edge detection method can be best explained by considering 1-D graphical illustrations as are presented in this section. Figure 4.3(a) shows a simple computer generated 2-D of size 20×120 pixels representing several step edges defining boundaries between regions of alternating gray scale intensities 102 and 204. The corresponding speckled image is obtained as described in section 3.3 and is shown in Figure 4.3(b).

1-D signals are obtained by extracting row #2 from *Bars* test image original of Figure 4.3(a) and speckled of Figure 4.3(b). A portion of the resulting 1-D signals, original and speckled are shown in Figure 4.4(A). The original pixel intensity scale of 0 – 255 gray levels is re-mapped in the graphs on to a scale 0 – 1 on y -axis in order to maintain consistent representation for the signals shown in the two graphs Figure 4.4(A) and 4.4(B). The MSPRoA algorithm described above for the natural 2-D domain is restricted here to vertical edges only in order to calculate edges for the 1-D signals, i.e. in this case the edge orientation is $O = 2$.

Figure 4.4(A) shows sampled 1-D test signal original $P(*, j)$ (indicated by \circ) and speckled (indicated by $*$) $S(*, j)$ extracted from test image *Bars* original (Figure 4.3(a))



(a)



(b)

Figure 4.3: Synthetic test image *Bars*

(a) Original; (b) Simulated speckled

and speckled (Figure 4.3(b)) respectively. From the graph shown in Figure 4.4(A) it can be seen that speckle exhibits signal dependent nature i.e speckle is significant in high intensity regions ($y = 0.8$) when compared to the low intensity regions ($y = 0.2$) for the speckled signal $S(*, j)$.

The ratio of averages edge strength value for speckled 1-D signal pixels $R(r)$ is calculated as explained in section 4.2.2 using mask size $N = 9$ and edge orientation $R(o) = 2$ indicating vertical edge condition. The corresponding $R(r)$ values plot is shown in Figure 4.4(B) (indicated by \times). A ratio threshold value of $T_r = 0.45$ is used to select candidate edge pixels $C(*, j)$. All the pixels for which $R(r)$ value is less than selected threshold value $T_r = 0.45$ are classified as candidate edge pixels. The corresponding candidate edge pixel locations $C(*, j)$ are shown in Figure 4.4(B) using \circ .

The pruning distance parameter $d = 2$ is used in pruning the candidate edge pixels. For $d = 2$ the D sub-window will have $((2d - 1) = 3)$ pixels. The pixels $P(*, j)$, $P(*, j - 1)$ and $P(*, j + 1)$ constitute the D sub-window pixels in this case. The pixel with maximum edge strength (the minimum $R(r)$) value is detected and labeled as $D(r)$. Pixel $P(*, j)$ is classified as edge pixel if it satisfied condition that $R(r) = D(r)$ and labeled as edge pixel $E(*, j)$. The corresponding MSPRoA edge pruned pixel locations are shown in the Figure 4.4(B) (indicated by \circ). All other pixels, i.e. pixels that were not selected as candidate pixels and the candidate pixels which does not satisfy maximum edge strength criteria are classified as non-edge pixels (not shown in the graph).

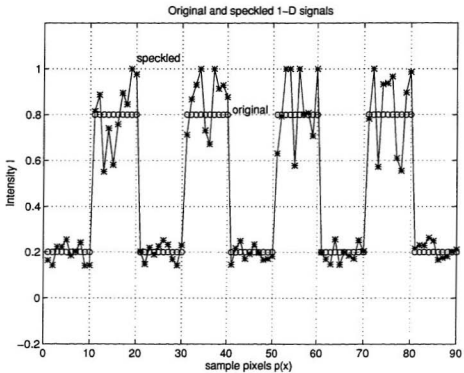


Figure 4.4: Illustration of the MSPRoA method using 1-D signals :
 (A): Original 1-D signal $P(*, j)[o]$; Speckled 1-D signal $S(*, j)[*]$.
 (Gray-scale intensity values 0 – 255 are remapped on to a 0 – 1 scale).

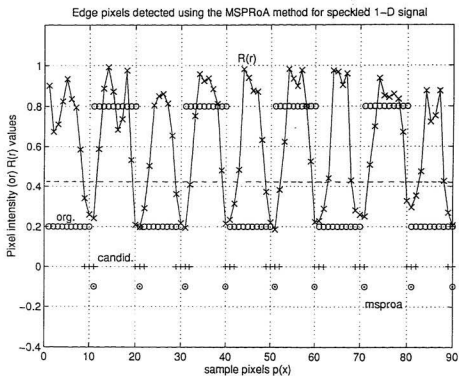


Figure 4.4 (B): Illustration of the MSPRoA method using 1-D signal:
 Original 1-D signal $P(*, j)[o]$; $R(r)$ values for speckled 1-D signal $[x]$;
 Threshold $T_r = 0.45$ value $[- -]$; The candidate edge pixels $C(*, j)[+]$;
 Locations of MSPRoA edge pixels for speckled 1-D signal $E(*, j)[o]$
 (Edge pixels locations are important and y - axis values not significant).

4.2.4 The effect of mask size (N)

As shown in Section 3.5.1 and Section 3.6, ratio based methods generate thick edge maps as mask size is increased. In this section the effect of mask size on the MSPRoA edge detection method is studied using 1-D test signal used in Section 4.1.3.

The MSPRoA method is used to obtain edge pixels from speckled 1-D signal of Figure 4.4(A) by varying the mask size for all odd values from $N = 5$ to $N = 11$. Figure 4.5 shows the 1-D signal of Figure 4.4(A) ($\{o\}$). The plot of $R(r)$ values, candidate edge pixels and the MSPRoA edge pruning pixels are obtained for each mask size. A ratio threshold value of $T_R = 0.4$ and correlation distance value $d = 2$ is used in each case. Figures 4.5(B), (C), (D) and (E) show corresponding the MSPRoA edge pixels plots for mask sizes $N = 5$ to $N = 11$ respectively. The $R(r)$ values calculated on speckled 1-D signal are represented using $[x]$. The candidate edge pixels $[+]$ and the MSPRoA edge pixels $[o]$ locations ($y - axis$ values are not significant) in the Figure 4.5 detected using different mask sizes.

From the test results in the Figures 4.5(A) to (E) show that, as mask size is increased the number of candidate edge pixels detected is increased which may be the reason for thick edge maps produced using previous methods. Based on experimental results, the MSPRoA method found to be successful in pruning the candidate edge pixels based on maximum edge strength values (i.e. minimum $R(r)$ values) generating precise and accurate edge maps giving edge pixels information close to the ideal edge pixels. Based on experimental results, the MSPRoA method has been found to be successful and consistent in producing thin and precise edge maps on speckled 1-D signal using different mask sizes.

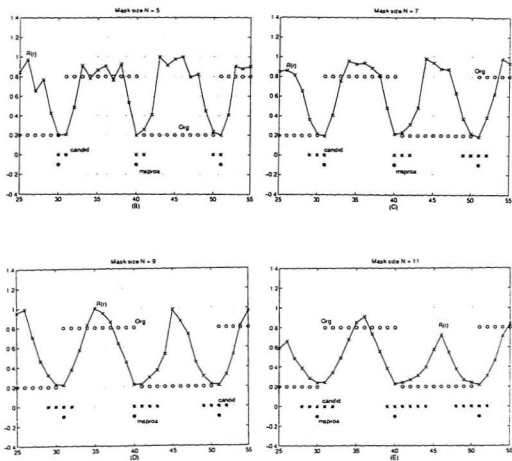


Figure 4.5: The effect of mask size on the MSPRoA method: (A) Original 1-D signal [o]; Speckled 1-D signal [+]; MSPRoA edge pixels for speckled 1-D signal using: (B) Mask $N = 5$; (C) Mask $N = 7$; (D) Mask $N = 9$; (E) Mask $N = 11$. (also shown $R(r)$ values [x]: Candidate edge pixels [+]).

4.2.5 The effect of correlation distance (d)

The MSPRoA method uses pruning distance parameter d value to select the D sub-window pixels used in pruning candidate edge pixels. In this section, the effect of correlating distance parameter d value on the MSPRoA edge detection method is studied and results are presented considering 1-D signals similar to those of 4.1.3.

Figure 4.6 shows a portion of an original 1-D test signal with step edges located at $P(\star, A)$, $P(\star, B)$, $P(\star, C)$, $P(\star, D)$, $P(\star, E)$, $P(\star, F)$, and $P(\star, G)$. Since edge pixels located at $P(\star, A)$, $P(\star, B)$ and $P(\star, E)$, $P(\star, F)$ are separated by only a few image pixels, these edges may represent very fine image detail. The remaining edge pixels ($P(\star, C)$, $P(\star, D)$, $P(\star, G)$) may represent medium or large structure detail. The corresponding speckled 1-D signal obtained using speckle noise model of Equation 2.29 is shown in Figure 4.6 using \star .

The MSPRoA method is used to extract edge pixels for the speckled 1-D signal using mask size $N = 9$, ratio-threshold $T_r = 0.45$ and with correlation distance varying from $d = 2$ to $d = 5$. Locations of the edge pixels $[o]$ detected using the MSPRoA method for different d values are shown in the graph (only locations are important, y - axis scale values not significant) of Figure 4.6.

According to the MSPRoA method the candidate edge pixel is selected as an edge pixel if its edge strength values $R(r)$ is minimum such values of all the pixels in the D sub-window. A value of $d = 2$ selects $(2 \times d - 1) = 3$ pixels or $P(\star, j \pm 1)$ pixels for the D sub-window over which the minimum $R(r)$ value is sought. For this value of d , the MSPRoA method is successful in detecting all true edge pixels, as no pixels in the neighborhood of $P(\star, j \pm 1)$ measured $R(r)$ values that are lower than the $R(r)$ values measured at $P(\star, j)$ locations.

For $d = 3$, sub-window D consists of $P(\star, j \pm 2)$ pixels. From the Figure 4.6, it can

be seen that the pixel located at $P(\star, B - 2)$ is found to be having $R(r)$ value which is less than the $R(r)$ value calculated for $P(\star, B)$ pixel. Hence, pixel $P(\star, B)$ is rejected as edge pixel using MSPRoA edge pruning. The use of $d = 4$ value found to have additional edge pixel located at $P(\star, E)$ rejected and, a value of $d = 5$ rejecting $P(\star, A)$, $P(\star, B)$, $P(\star, C)$, $P(\star, E)$ and $P(\star, F)$ edge locations.

The use of correlation distance value $d = 2$ was found to be successful in extracting true edge pixel information on both images having fine and large structure. The use of large d values ($d \geq 4$) was found to result in true edge pixels being missed on fine details. A large d value was found to be acceptable in case of moderate or large image structure. However, the use of large d values may increase computational costs required in measuring $D(r)$ values. The correlation distance value $d = 1$ provides edge maps with no edge pruning (since D sub-window consists of only one pixel), and is equivalent to the MRoA edge detector.

Study and analysis of correlation distance effect on the MSPRoA method using 1-D test signal show that the MSPRoA method is sensitive to the correlation distance d value. This parameter value must be carefully selected with a view to the underlying image structure. A value of $d = 2$ for images that consists of fine detail. The use of larger values $d \geq 4$ is found to be acceptable for achieving edge pruning without loosing fine details information. For most of the applications a value of $d = 2$ or $d = 3$ provides both edge pruning and also computational savings.

4.3 A 2-D example

The MSPRoA edge detection method is tested using 2-D *Bars* test images. The ideal edge map for the noise-free *Bars* image of Figure 4.3(a) is obtained using Sobel

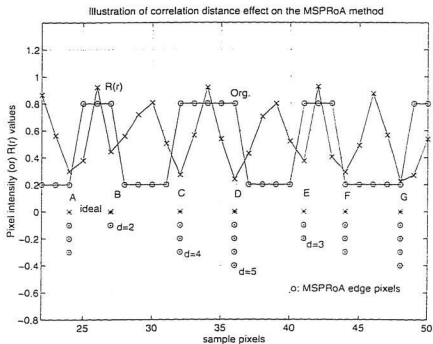


Figure 4.6: The effect of correlation distance d on the MSPRoA method
Original 1-D signal [o], $R(r)$ values [x] and the MSPRoA edge pixels [o] computed on speckled 1-D signal using $N = 9$, $T_r = 0.45$, and d values from $d = 2$ to $d = 5$.

The MSPRoA edge detector quantitative performance evaluation measures computed using edge maps for 2-D *Bars* .

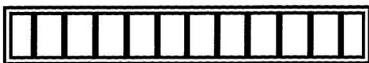
Test Image	Edge Operator	N	T_s	T_r	$\#found$	C in %	M in %	W in %	A in %
Original	Sobel	3	20	-	308	100.0000	0.0000	0.0000	0.0000
Speckled	MSPRoA	13	-	0.65	154	132.4675	0.0000	0.0000	0.6493

Table 4.1: The MSPRoA performance evaluation for test image *Bars*

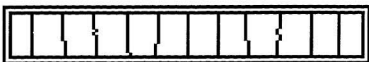
$$C = \frac{2 \times \#correct}{\#true + \#found} ; M = \frac{\#mis}{\#true} ; W = \frac{\#wrong}{\#true} ; A = \frac{\#ambig}{\#true} .$$

operator of Equation 2.6 is shown in Figure 4.7(a). The MSPRoA edge map on the speckled *Bars* of Figure 4.3(b) is obtained using mask size $N = 13$, ratio threshold $T_r = 0.63$ and correlation distance $d = 2$, and is shown in Figure 4.7(b). The edge detector quantitative performance evaluation measures of Section 3.2.2 are calculated from the edge map obtained using the MSPRoA method and are listed in Table 4.1.

The original *Bars* test image shown in Figure 4.3(a) of size 20×120 consists of 11 step edges and a $\#3 - pixel$ border. If the border pixels are excluded $2 \times 3 - pixels = 6 - pixels$ which does not include any edge pixel information the *Bars* image will be of the size 14×114 . The total number of true edge pixels measured will be equal to $11 \times 14 = 154$. Hence an edge detector must detect 154 edge pixels arranged into 11 strips each consisting of 14 pixels each.



(a)



(b)

Figure 4.7: The MSPRoA edge detection test results on *Bars*
(a) Sobel edge map on original [$T = 20$]; (b) The MSPRoA edge map
for speckled *Bars* [$N = 15$, $T_r = 0.64$, $d = 2$].

The Table 4.1 shows that the Sobel operator on the original *Bars* image detected the *#found* edge pixels equal to 308 and 11 strips, hence the edge map which is a two pixels wide ($2 \times 154 = 308$). The MSPRoA edge map on speckled *Bars* image detected edge map with the *#found* edge pixels and 11 strips and hence is, relative to the Sobel operator, only one pixel wide ($1 \times 154 = 154$).

The quantitative performance measures *C*, *W*, *M*, and *A* measured on the MSPRoA edge map are all close to their ideal edge map parameter values. The qualitative evaluation of MSPRoA method for speckled *Bars* test image show that the method gives close approximation to the corresponding ideal edge map obtained on noise-free *Bars* test image. However, these values are some what misleading, due to the fact that the Sobel edge map is two pixels wide. In fact, it can be visually noted in Figure 4.7(b) that the MSPRoA is jagged within that 2-pixel width.

The MSPRoA method detected edge map on 2-D speckled *Bars* test image with single pixel accuracy. The method found to be successful in obtaining edge map on speckled image which is thin and precise giving close estimation to the corresponding ideal edge map. The method also found to be successful suppressing spurious edge pixel information in homogeneous regions. The edge detector quantitative performance evaluation measures obtained on the MSPRoA edge map measured values close to the ideal edge map measures. However, a few edge pixels detected using the MSPRoA methods are off the track and showed some deviations when compared with the ideal edge maps.

Overall, the MSPRoA method tested using the 1-D test signals and the 2-D *Bars* image was found to be successful in generating precise and accurate edge maps on speckled signals. The edge pixel detected for the speckled 1-D signal and 2-D image using the MSPRoA method are close to the corresponding ideal edge pixels, as reflected

by their quantitative performance measures.

Using this knowledge and information the MSPRoA method is further tested in Chapter 5, both synthetic and real 2-D test images in order to further investigate its performance on speckled images. The MSPRoA edge detection test results, comparative study and discussion of the results based on both quantitative and qualitative methods is presented in the next Chapter.

Chapter 5

Results and Discussion

5.1 Introduction

In this chapter, MSPRoA edge detection test results on 2-D speckled test images are presented together with discussion analyzing the performance of the MSPRoA method on speckled images. Several 2-D test images are considered for the purpose of study and analysis including both synthetic and real airborne SAR images of varying scene contents. The results of MSPRoA edge detection on speckled images are evaluated using qualitative and quantitative methods. A comparative study and analysis of the MSPRoA edge detection method and of previous speckle specific edge detection methods is conducted.

The test results and discussion presented in this chapter are mainly divided into two groups. In the first group, test results for synthetic test images of varying scene contents are presented and discussed. The MSPRoA edge detection results on these synthetic test images are evaluated using qualitative and quantitative performance measures and compared with similar results obtained for these test images in Chapter [3] by previous speckle specific edge detection methods.

In the second group, the MSPRoA test results using airborne SAR images are considered. Several test images, some of which previously used in Chapter [3] are considered for test and discussion. Edge maps generated from these real SAR images are evaluated using qualitative analysis only since in this case ideal edge maps are unavailable. The performance of the MSPRoA method on the real airborne SAR images is compared to that of previous speckle specific edge detector methods.

A fast edge tracking algorithm to improve the visual quality of the edge maps generated by the MSPRoA method is suggested. The MSPRoA edge tracking algorithm is tested on the synthetic and real airborne SAR test images and the test results are presented. An analysis of test results using the MSPRoA edge tracking algorithm is conducted.

The use of the MSPRoA algorithm at multiple scales is also addressed in order to deal with the problem of extracting edge information from both fine and large structures on speckled images. A simple multi-scale MSPRoA algorithm is suggested which can extract true edge information at multiple scales. Performance of the multi-scale MSPRoA algorithm is studied using the synthetic and real airborne SAR speckled test images.

5.2 The MSPRoA on synthetic test images

The synthetic test images *Strips* (Figure 3.2(a)), *Ring*(Figure 3.3(a)), and *Combine* (Figure 3.4(a)) and corresponding simulated speckled images, used in Chapter [3] are used again here for the study and analysis of the MSPRoA method. Edge maps obtained by applying the MSPRoA method on corresponding speckled images for *Strips*, *Ring* and *Combine* are presented. The performance of the MSPRoA edge detection method for such speckled images is studied and analyzed by using qualitative and quantitative

methods.

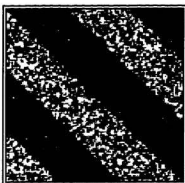
The synthetic speckled image *Strips* (Figure 3.2(b)) and corresponding Sobel (Equation 2.6) ideal edge map obtained on noise-free image (Figure 3.9(c)) are shown here in Figures 5.1(a) and Figure 5.1(b). The MSPRoA edge map on speckled *Strips* is obtained using $N = 15$, $T_r = 0.63$ and $d = 2$ and is shown in Figure 5.1(c). The MSPRoA edge map for speckled *Strips* is over laid on the ideal edge map for noise-free image to compare the MSPRoA detected edge pixel edge localization with respect to ideal edge pixels and is shown in Figure 5.1(d). In Figure 5.1(d), the MSPRoA edge pixel are shown using white pixels, the ideal edge pixels are shown using black pixels on a light-gray background.

Similar tests were conducted for the test image *Ring* and are shown using Figures 5.2(a) to (d). The MSPRoA method is also tested on *Combine* test image which included *Strips*, *Ring* and an outdoor scene *Balloon*. The MSPRoA test results for *Combine* test image are shown in Figures 5.3(a) to (d). The corresponding MSPRoA edge maps for *Ring* and *Combine* are obtained using $N = 13$, $T_r = 0.66$, $d = 2$ and $N = 13$, $T_r = 0.63$ and $d = 2$, respectively.

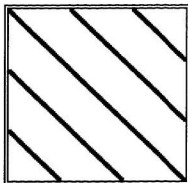
5.2.1 Qualitative analysis of MSPRoA results on synthetic images

Edge detection results obtained using the MSPRoA method are evaluated qualitatively mainly based on human perception. Edge maps obtained using the MSPRoA method are compared with the corresponding ideal edge maps obtained under noise-free conditions to evaluate how close the MSPRoA edge maps are to ideal conditions edge maps.

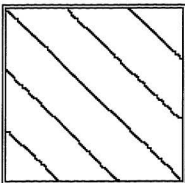
The MSPRoA edge map for the test image *Strips* (Figure 5.1(c)) shows that the



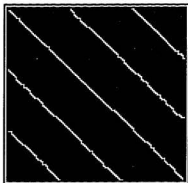
(a)



(b)



(c)



(d)

Figure 5.1: The MSPRoA test results on synthetic test image *Strips* :
(a) Speckled *Strips* ; (b) Sobel edge map for Figure 3.2(a) [$T=20$] ;
(c) The MSPRoA edge map for (a) [$N = 15$, $T_r = 0.63$, $d = 2$] ;
(d) Edge map (c) in white pixels overlaid on (b) in black pixels.

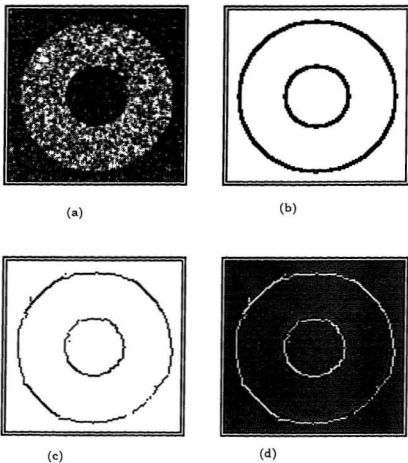
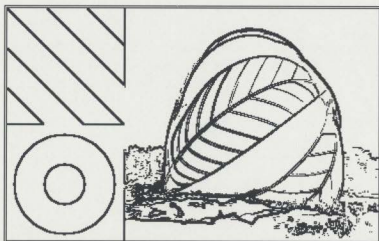


Figure 5.2: The MSPRoA test results on synthetic test image *Ring* :
 (a) Speckled *Ring* ; (b) Sobel edge map on Figure 3.3(a) [$T=20$];
 (c) The MSPRoA edge map on (a) [$N = 13$, $T_r = 0.66$, $d = 2$];
 (d) Edge map (c) in white pixels overlaid on (b) in black pixels.

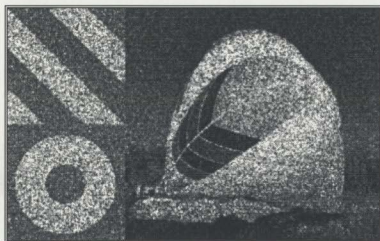


(a)

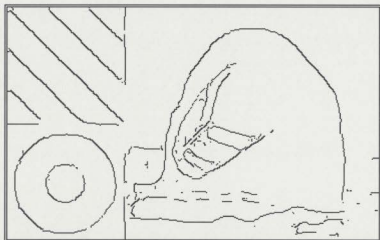


(b)

Figure 5.3: The MSPRoA test results on test image *Combine* :
(a) Original *Combine* ; (b) Sobel edge map for (a) [$T=100$].



(c)



(d)

Figure: 5.3 The MSPRoA test results on test image *Combine*: (c) Speckled *Combine* ;
(d) The MSPRoA edge map for (c) [$N = 13$, $T_r = 0.63$, $d = 2$].

method is successful in generating thin and localized edges from the corresponding speckled image yielding an edge map which approximates closely to the ideal edge map (Figure 5.1(b)). The method is also successful in suppressing spurious (wrong) edge pixels detected in homogeneous (non-edge) regions. There are no true edge pixels that are missing when compared with the ideal edge map. Overall, these test results confirm that the MSPRoA method is successful for the speckled *Strips* image in generating an edge map giving close approximation to the ideal edge map.

The MSPRoA method on the test image *Ring* also generated an edge map for the speckled image which is close to the corresponding ideal edge map. There are few and / or no spurious (wrong) edge pixels detected in homogeneous (non-edge) regions. The generated edge map is thin and precise. However, a few edge pixels in the ideal edge map are missing in the corresponding MSPRoA edge map giving rise to discontinuities in the detected edge contours. Overall, the MSPRoA test results on the speckled *Ring* test image shows that the method generated a thin and precise edge map which is a close approximation to the ideal edge map (Figure 5.2(b)).

Test results on the *Combine* show that the MSPRoA detected a clean and precise edge map for the speckled image, suppressing spurious edge responses in homogeneous regions. Regions and boundaries between regions are well defined in the generated edge map. However, visual examination show that several true edge pixels in the ideal edge map are missing in the corresponding MSPRoA edge map. Fine detail and low contrast information, particularly in the balloon, are missing in the MSPRoA edge map. Overall, the MSPRoA generated edge map shows well-defined object and regions boundaries with few spurious edges in non-edge regions, but with several true edge pixels missing in area which are finely detailed or of low contrast.

The above test examples confirm that the MSPRoA method can be successful in gen-

erating thin and localized edge maps without the necessity of either gradient information calculations or edge thinning post processing.

5.2.2 Quantitative analysis of MSPRoA results on synthetic images

The MSPRoA edge detection results for synthetic test images are evaluated using the edge detector quantitative performance evaluation measures proposed by Zaman and Moloney (section 3.2.2). These evaluation results computed from the edge maps of *Strips*, *Ring* and *Combine* are shown in Table 5.1.

The MSPRoA edge detector quantitative performance evaluation results shown in Table 5.1 confirm that the MSPRoA method is successful in extracting edge maps on speckled images with quantitative performance measures close to those of the corresponding ideal edge maps. The results for test images *Strips* and *Ring* indicate performance close to their ideal edge map measures. In the case of the third test image *Combine* the quantitative performance measures were found to be better in terms of edge pixel correctness (high C), better suppression of spurious edge pixels (low W) and good localization as indicated by low ambiguity (low A) values. However, the edge map missed a number of true edge pixel information (high M) which is an undesirable performance measure.

Regions on the balloon in the central part of *Combine* consists of several fine details in two differing shades of gray. Due to the signal dependent nature of speckle noise, the interfering noise is more significant in the lighter gray regions compared to the darker gray regions. Speckle noise in the balloon central gray shaded region severely degraded the underlying image information making it difficult to extract information from this region.

Image Sample	Edge Operator	Figure	MSPRoA parameters	#found	C in %	M in %	W in %	A in %
<i>Test Image Strips</i>								
Original	Sobel	5.1(b)	T=20	1308	100.00	0.00	0.00	0.00
Speckled	MSPRoA	5.1(c)	N=15 Tr=0.63 d=2	652	100.00	0.30	0.00	0.38
<i>Test Image Ring</i>								
Original	Sobel	5.2(b)	T=20	1128	100.00	0.00	0.00	0.00
Speckled	MSPRoA	5.2(c)	N=13 Tr=0.66 d=3	465	100.00	8.86	0.21	7.80
<i>Test Image Combine</i>								
Original	Sobel	5.3(b)	T= 80	13556	100.00	0.00	0.00	0.00
Speckled	MSPRoA	5.3(c)	N=13 Tr=0.63 d=2	3038	73.07	50.32	2.86	4.94

Table 5.1: The MSPRoA edge detector quantitative evaluation measures

If the original noise-free image were not available the human viewer might also fail to extract some of the true edges from this region. Information in the darker gray region in the central part of the balloon was also partly degraded by the interfering speckle noise but a good edge detector could be expected to extract at-least some of the underlying image information. The edges in this region were detected by the MSPRoA method but may consists of missing pixels information when compared with the human perceived edge map.

Overall, the MSPRoA method was found to be successful in extracting true edge information from speckled images having medium to large structures (e.g. *Strips. Ring*) with performance measures close to that of the ideal edge maps. The MSPRoA method was satisfactory on a test image having a variety of scene contents (e.g. *Combine*). For all the test images used, the MSPRoA method generated edge maps were thin and precise without requiring edge thinning post processing operations or gradient calculations. However, the method performed relatively poorly in extracting the edges of fine details from images when image consisted of fine, medium and large structures information, especially in regions of low image contrast and significant speckle.

These test results using 2-D synthetic test images confirmed the suitability of the MSPRoA method for detecting edges in speckled image. Therefore, with knowledge gained about the method's performance and appropriate parameter setting, the study of the MSPRoA method continued with SAR test images.

5.3 The MSPRoA on airborne SAR images

5.3.1 Test Results

SAR test images *Fields* (Figure 5.4(a)), *Busy* (Figure shown here Figure 5.5(a)), *Industrial* (Figure 5.7(a)) and *Highway* (Figure 5.6(a)) are used for test and analysis of the MSPRoA edge detector performance on real airborne SAR images.

SAR test image *Fields* consists of woods and fields areas and is similar to test image *Moderately Busy* (Figure 3.5) shown in Chapter [3]. This test image is an example of a SAR image containing several low and high contrast regions and with large structures. An MSPRoA edge map is obtained on the SAR test image *Fields* using mask size $N = 9$, ratio threshold $T_r = 0.6$ and correlation distance value $d = 2$. The resulting edge map is shown in Figure 5.4(b).

Test image *Busy* contains predominantly fine structures and is "busy" as a consequence. The underlying image is a suburban city area, which has several straight roads and rows of houses in the ordered manner of man-made structures. The edge map obtained using the MSPRoA method on the *Busy* SAR test image is shown in Figure 5.5(b). The edge map was generated using mask size $N = 9$, ratio threshold $T_r = 0.62$ and $d = 2$ correlation distance parameter value.

The test image *Highway* (Figure 5.6(a)) contains information on highway roads and small objects such as cars on the highways which can all be classified as fine structures. The test image *Highway* also contains some fields which are large structures. This test image also suffers from a relatively poor contrast ratio sometimes observed in SAR images. Figure 5.6(b) shows the MSPRoA edge map on the test image *Highway* obtained using mask size $N = 7$, ratio threshold value $T_r = 0.6$ and correlation distance parameter value $d = 2$.

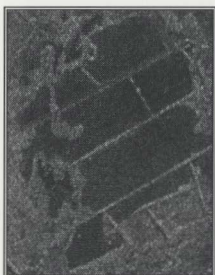
Test image *Industrial* (Figure 5.7(a)) is SAR image containing fine, large and medium structures varying from region to region. Test image *Industrial* is included as an example of an image containing both very busy and moderately busy regions in one image. Figure 5.7(b) shows the MSPRoA edge map on *Industrial* test image. This edge map was obtained using mask size $N = 11$, ratio threshold value $T_r = 0.63$ and correlation distance value $d = 2$.

5.3.2 Analysis of MSPRoA test results on SAR Images

The above edge detection results on real airborne SAR images of varying scene contents confirm the suitability of the MSPRoA method for use on real speckled images. The test results also show that the MSPRoA method can be successful in generating thin and precise edge maps on real SAR images.

The MSPRoA edge map on the test image *Fields* resulted in well defined boundaries between regions with few spurious edges in non-edge regions (Figure 5.4(b)). Test results obtained on the SAR test image *Busy* also found thin and precise edges with a small number of wrong edge pixels. The corresponding edge map also conveys some information about the underlying image objects as the edge map consists of well defined rows indicating the possibility that the regions may correspond to an area of man-made structures such as the houses and the streets found in cities.

Test results on the SAR test image *Highway* also resulted in well defined edge map confirming suitability of the MSPRoA method for detecting edges on speckled images. The MSPRoA edge map (Figure 5.6(b)) on SAR test image *Highway* successfully extracted edges information on fine details such as closely located highway roads. Information on large structures in the regions on either side of the highway roads are also well registered with clean boundaries defined. Fine objects such as cars on highway roads



(a)



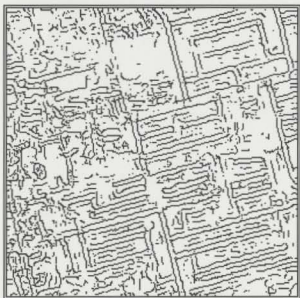
(b)

Figure 5.4: The MSPRoA test results on SAR test image - *Fields* :

(a) SAR image *Fields*; (b) MSPRoA edge map for (a) [$N = 9$, $T_r = 0.6$, $d = 2$].



(a)



(b)

Figure 5.5: The MSPRoA test results on SAR test image *Busy* :
(a) SAR image *Busy* ; (b) MSPRoA edge map for (a) [$N = 9$, $T_r = 0.62$, $d = 2$].



(a)

Figure 5.6: The MSPRoA test results on SAR test image *Highway* :

(a) SAR test image *Highway* ;



(b)

Figure 5.6: The MSPRoA test results on SAR test image *Highway*:

(b) The MSPRoA edge map for (a) [$N = 7$, $T_r = 0.6$, $d = 2$].



(c)



(d)

Figure 5.6: The MSPRoA test results on SAR image *Highway* :
(c) A zoom out from 5.6(a); (d) A zoom out from 5.6(b).



(a)



(b)

Figure 5.7: The MSPRoA test results on SAR test image *Industrial* :
(a) SAR test image *Industrial* ; (b) The MSPRoA edge map for (a)
using $[N = 11, T_r = 0.63, d = 2]$.

could be clearly seen in extracted edge map. A zoom out of the MSPRoA edge map on *Highway* is shown in Figure 5.6(d).

Analysis of the test results on SAR test image *Industrial* shows that the MSPRoA method also extracted edge maps for this test image, suppressing spurious edge responses in homogeneous (non-edge) regions. True edge pixel information was successfully registered from the regions consisting of fields and roads. However, boundaries were poorly defined in the middle portion of the image consisting of the man-made structures of a large industrial complex (Figure 5.7(a)). The MSPRoA edge map included relatively more spurious edges in this region compared to the other regions of the *Industrial* test image.

The MSPRoA edge detection test results on real airborne SAR images confirmed the test results observed on synthetic test images. The MSPRoA method was also found to be successful on real SAR images in generating thin and localized edge maps without requiring gradient calculations or edge thinning post processing. The performance of the MSPRoA method was found to be satisfactory on images having large, moderate, fine and/ or busy structures as observed from test results on *Fields*, *Busy* and *Highway*. The method was also found to be successful in extracting information from images having a variety of scene contents and poor contrast such as the *Highway* test image. However, the method performed relatively poorly on test image *Industrial* which contains a variety of image structures.

5.4 Discussion

5.4.1 Comparative study using synthetic test images

A comparative study and analysis of the MSPRoA edge detection method and of previous speckle-specific edge detection methods is conducted in this section, based on results obtained using synthetic test images. The speckle specific edge detection methods previously investigated to in Chapter 3, are studied again, in terms of determining how close their quantitative performance measures can be to the ideal conditions values.

The test image *Strips* is first considered for this study and analysis. We attempt first to optimize each edge detector's quantitative performance measure W (Equation 3.5) determining the number of wrong edge pixel information. Edge maps are obtained which yield the W performance measure close to the ideal conditions value (i.e. $W = 0$) using different edge detection methods. The corresponding quantitative performance measures M (Equation 3.4), A (Equation 3.3) and C (Equation 3.2) are measured. These values indicating the performance of different edge detectors are shown in Table 5.2. Similar tests conducted to optimize primarily M and A and the corresponding test results are shown in Table 5.3 and Table 5.4, respectively.

As seen from Table 5.2, attempts to achieve values of the edge detector measure W close to the ideal condition of $W = 0$ found to be successful using the previously studied speckle specific edge detection methods. The resulting edge maps also have their performance measures close to ideal edge map values in terms of edge *correctness* and *ambiguity* which measured high C and low A values. However, the edge maps missed a number of true edge pixels as seen by their high M values. Therefore, the existing speckle specific edge detection methods resulted in poor edge maps in terms of missing true edge pixel information when an attempt is made to optimize the number

Test Sample	Edge Detector	Mask N	Threshold		#found	C in %	M in %	W in %	A in %
			T_p	T_r					
Test Image Strips									
Original	Sobel	-	20	-	1308	100.00	0.00	0.00	0.00
..	Coeff.	7	-	0.42	166	23.06	79.28	1.80	7.72
..	Touzi	9	-	0.55	627	95.29	23.08	0.00	6.42
..	RoA	5	-	2.35	201	69.18	56.80	0.00	3.28
..	MRoA	7	-	0.55	554	100.00	25.61	0.00	3.21
..	RGoA	7	85	0.52	600	98.63	23.39	0.00	4.66

Table 5.2: Optimizing edge detector quantitative performance measure W

of *wrong* edge information.

Test measures optimizing M were found to be satisfactory using the Touzi, MRoA and RGoA methods in terms of their M and W measure. However, the results showed poor performance measures in terms of edge *correctness* (C) and *ambiguity* (A) values. Therefore, the existing edge detection methods performed poorly when attempts were made to extract all true edge pixel information. The generated edge maps measured a number of *ambiguous* edge pixels and showed poor *correctness*.

The test results for optimizing the edge *ambiguity* ($A \approx 0$) are shown in Table 5.4. The edge detector performance measure A is important as it indicates a measure of closeness between a detected edge map and its ideal edge map. It also indicates a measure of edge localization. Thick edge maps in general measure high A values indicating poor edge localization Table 5.4 shows that the resulting edge maps for the MRoA and RGoA methods have their performance measures W and C values close to the ideal edge map values. However, the edge maps also have high M values indicating

Test Sample	Edge Detector	Mask N	Threshold		#found	C in %	M in %	W in %	A in %
			T_f	T_r					
Test Image Strips									
Original	Sobel	-	20	-	1308	100.00	0.00	0.00	0.00
..	Coeff.	7	-	0.28	2353	20.70	0.45	17.33	70.56
..	Touzi	9	-	0.69	2042	25.31	0.00	6.41	67.58
..	RoA	7	-	1.69	3231	7.49	0.00	32.52	87.00
..	MRoA	13	-	0.63	1737	32.44	0.00	1.15	62.23
..	RGoA	13	85	0.62	1691	43.68	0.00	1.47	49.92

Table 5.3: Optimizing edge detector quantitative performance measure M

that these edge maps miss a number of true edge pixels and hence a relatively poor match to ideal edge maps is achieved. Other previous speckle specific edge detector performance measures show relatively poor performance measures both in terms of edge *correctness* (low C values) and *missing* true edge pixels (high M values) and hence indicate poor performance compared to MRoA and RGoA methods.

The performance measures of the existing speckle specific edge detection methods are compared with the performance measures of the MSPRoA method for the *Strips* test image listed in Table 5.1. The measured performance measures show that the previous speckle specific edge detection methods could achieve performance measure values close to the values measured on ideal edge maps only with one parameter selected at any time. Attempts to improve any one of the performance measure value were found to influence other measures, modifying their measures in an undesirable manner.

The MSPRoA results (Table 5.1) show that the method achieved performance measures C , M , W and A all close to their ideal edge map value simultaneously. Therefore.

Test Sample	Edge Detector	Mask N	Threshold		#found	C in %	M in %	W in %	A in %
			T_g	T_r					
<i>Test Image Strips</i>									
Original	Sobel	-	20	-	1308	100.00	0.00	0.00	0.00
..	Coeff.	5	-	0.44	56	21.99	86.54	3.57	1.98
..	Touzi	7	-	0.48	157	59.38	66.05	0.00	0.68
..	RoA	7	-	2.4	75	29.79	82.26	1.33	1.98
..	MRoA	7	-	0.52	345	87.87	45.02	0.00	0.42
..	RGoA	7	85	0.52	385	90.49	39.52	0.00	1.91

Table 5.4: Optimizing edge detector quantitative performance measure A

the MSPRoA method is successful on the test image *Strips* achieving performance measures close to its ideal edge map performance measure values.

Overall, the MRoA and RGoA methods resulted in better performance relative to the other previous speckle specific edge detection methods. Hence these edge detection methods are selected for comparative study and analysis of the MSPRoA edge detection results using qualitative analysis.

Figure 5.8(a) shows the ideal edge map obtained on *Strips* noise-free image using Sobel operator. Figure 5.8(b) shows the MRoA edge map obtained using mask size $N = 7$, threshold value $T = 0.62$ followed by edge thinning. Figure 5.8(c) shows the RGoA edge map obtained using mask size $N = 9$, ratio threshold $T_r = 0.6$ and gradient threshold $T_g = 65$ followed by edge thinning. Figure 5.8(d) shows the MSPRoA edge map obtained using mask size $N = 15$ ratio threshold $T_r = 0.63$ and correlating distance $d = 2$. The corresponding edge maps for the *Ring* and *Combine* images are also obtained. Figures 5.9(a) to (d) show these edge maps for the *Ring* and Figures 5.10(a) to (d) show

edge maps for the *Combine* image.

This comparative study and analysis of the edge maps obtained using the MRoA, RGoA and MSPRoA methods show that the edge maps obtained using the MSPRoA method are relatively better compared to the edge maps obtained using previous edge detection methods. Edge maps obtained using the MSPRoA method are well defined with continuous lines between regions (test results on *Strips* and *Combine*). The suppression of spurious edge pixel information is also relatively better using the MSPRoA method as seen from the *Strips*, *Ring* and *Combine* edge maps. The MSPRoA method was also found perform well on *Ring*, the edge map of which contains changing edge orientations.

Qualitative analysis of the test results these on synthetic test images also show that the MSPRoA method performed better in detecting edges on speckled images as compared to the existing edge detection methods. The MSPRoA edge maps obtained on speckled images are seen to be precise and accurate. These edge maps suppress spurious edge pixel information relatively better compared to edge detection methods. The edge maps are also continuous and successful in giving well defined boundaries between regions. These test results encourage the use of the MSPRoA method for detecting edges on speckled images.

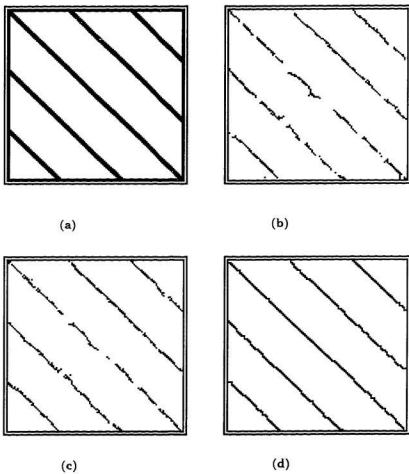


Figure 5.8: The MSPRoA test results a comparative study using *Strips* :
 (a) Sobel for original [$T=20$] ; (b) MRoA for speckled [$N = 7$, $T_r = 0.65$] followed by edge thinning; (c) RGoA for speckled [$N = 9$, $T_r = 0.65$, $T_s = 75$] followed by edge thinning; (d) MSPRoA for speckled [$N = 15$, $T_r = 0.63$, $d = 2$].

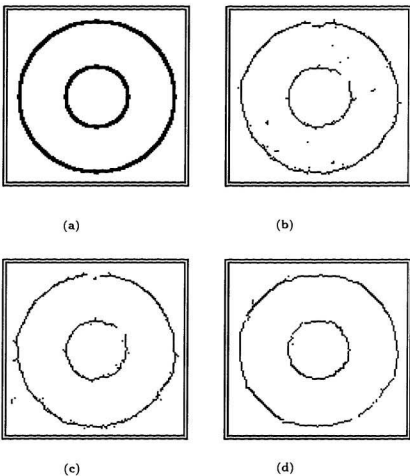
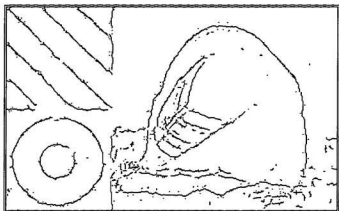
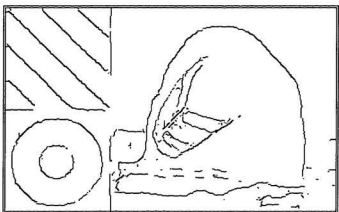


Figure 5.9: The MSPRoA test results a comparative study using *Ring* :

- (a) Sobel for original [$T \approx 20$]; (b) MRoA for speckled [$N = 7$, $T = 0.65$] followed by edge thinning; (c) RGoA for speckled [$N = 7$, $T = 0.65$, $T_s = 85$] followed by edge thinning; (d) MSPRoA for speckled [$N = 13$, $T = 0.66$ and $d = 2$].



(a)



(b)

Figure 5.10: The MSPRoA method a comparative analysis using *Combine* :
 (a) RGoA for speckled [$N = 7$; $T_r = 0.58$; $T_g = 85$] followed by edge thinning;
 (b) MSPRoA for speckled [$N = 13$; $T = 0.62$; $d = 2$].

Test Image	Edge Detector	Mask N	Threshold		#found	C in %	M in %	W in %	A in %
			T_r	T_g					
Original	Sobel	-	20	-	1308	100.00	0.00	0.00	0.00
Speckled	MRoA	5	0.58	-	747	100.00	14.52	9.50	5.73
..		7	0.59	-	851	94.48	11.77	0.70	10.24
..		9	0.59	-	971	90.21	8.33	0.30	13.07
..		11	0.59	-	1120	82.20	5.04	0.44	18.65
..		13	0.59	-	1237	69.39	5.81	0.32	26.68
..	RGoA	5	0.53	85	602	98.74	22.62	5.64	5.27
..		7	0.55	85	675	97.42	19.26	0.29	6.88
..		9	0.57	95	833	89.49	12.99	0.24	13.76
..		11	0.57	95	943	85.07	9.40	0.00	17.35
..		13	0.57	95	1069	76.81	7.11	0.00	23.08
..	MSPRoA	5	0.60	d=2	578	100.00	9.70	8.13	3.59
..		7	0.61	..	590	100.00	4.89	0.33	2.75
..		9	0.61	..	614	100.00	3.59	0.32	1.45
..		11	0.63	..	650	100.00	0.91	0.15	1.52
..		13	0.63	..	654	100.00	0.38	0.00	0.61

Table 5.5: The effect of mask size on MSPRoA edge detector

5.4.2 Study on the effect of mask size

The effect of mask size on 1-D test signal is studied in Chapter [4]. Further, study on the effect of mask size on the MSPRoA method using 2-D test images is conducted and presented in this section. Test images *Strips*, *Ring* and *Combine* where the corresponding ideal edge maps are available are used for study and analysis purpose.

Edge maps are obtained on test images *Strips*, *Ring* and *Combine* using MRoA, RGoA and the MSPRoA methods by varying mask size from $N = 5$ to $N = 13$. Quantitative performance measures computed each case using Zaman and Moloney edge detector

performance measures (section 3.2.2). Test results showing performance measures for different mask sizes are shown in Table 5.5.

From the table it can be seen that as the mask size is increased from $N = 5$ to $N = 13$ edge detector performance measures M and W are improved for all the three methods (ex. MRoA: $M = 14.52$ to $M = 5.81$, RGoA: $M = 22.62$ to $M = 7.11$ and MSPRoA: $M = 9.7$ to $M = 0.38$). However, the edge detector performance measures C and A values are deteriorated as the mask size is increased in case of MRoA and RGoA methods. In case of MRoA method as the mask size is increased C value reduced from $C = 100$ to $C = 69.39$ and corresponding A values increased from $A = 5.73$ to $A = 26.68$. Similar effect could be observed in case of RGoA method. In this case the corresponding values found to be changed from $C = 98.74$ to $C = 76.81$ and $A = 6.88$ to $A = 23.08$. In case of the MSPRoA method increase in mask size found to be improving A value (from $A = 3.59$ to $A = 0.61$) without effecting C value.

The use of small mask sizes found to be better suited for extracting edge maps with high correctness C values. However, these edge maps also measured high W and M values. The use of large mask sizes found to be useful in improving W and M values however, it has a negative effect on corresponding C and A values in using MRoA and RGoA method. In case of MSPRoA method the use of large mask size found to be useful in extracting in extracting number of true edge pixels without effecting other parameter values in an undesirable manner. However, it is not recommended to use very large mask sizes as it may increase computational costs in measuring edge strength magnitude values.

5.4.3 Comparative study and analysis using SAR images

A comparative study and analysis of the MSPRoA edge detection results using airborne SAR images is presented in this section. The MRoA and RGoA edge detection methods are selected for comparison with the MSPRoA method as these methods reported better performance of the existing methods. The standard MRoA thinning algorithm is used to produce thin and precise edge maps for the MRoA and RGoA methods which can be compared with the MSPRoA edge maps.

Figure 5.11(a) shows the SAR test image *Fields*. Figure 5.11(b) shows the MRoA edge map on *Fields* obtained using mask size $N = 7$, ratio threshold $T_r = 0.45$ followed by edge thinning. The RGoA edge map, obtained using mask size $N = 9$, ratio threshold $T_r = 0.45$, gradient threshold $T_g = 50$ followed by edge thinning, is shown in Figure 5.11(c). The MSPRoA edge map obtained using mask size $N = 9$, threshold $T = 0.6$ and correlation distance $d = 2$ is shown in Figure 5.11(d). The MSPRoA edge map with parameters used in Figure 5.5(b) is shown in Figure 5.12(d) for comparison purpose. Similar tests conducted on *Highway* and *Industrial* and test results with corresponding operating parameters are shown in Figures 5.13 and Figures 5.14 respectively.

From the figures it can be seen that the MSPRoA generated edge maps are thin and more complete when compared to the MRoA or RGoA generated edge maps. The figures also show that the MSPRoA method generated edge maps for these SAR images are of better quality than those generated by the MRoA or RGoA methods as the boundaries are well defined and lines are continuous for all the test images. The MSPRoA method achieved improved performance without requiring edge thinning operations.

Although the edge map for the test image *Moderately Busy* missed several edge pixels, the MSPRoA generated edge map indicates well defined regions compared to the edge maps of the other two methods. Similar results are observed in the case of the *Busy*

test image. The edge map generated using the MSPRoA method resulted in a greater number of true edge pixels detected the lanes appearing in the original SAR images are well registered using the MSPRoA method. The suppression of false edge pixels in homogeneous regions is also better for this SAR image compared to the RGoA and MRoA methods.

The performance of the MSPRoA method was found to be successful for the test image *Highway*. Roads and boundaries between regions in the fields are well registered using the MSPRoA method. The small objects visible on the roads which may indicate moving cars were also registered using the MSPRoA edge detection method. The generated edge map was also found free from false edge pixels.

The test results on *Industrial* image are shown in Figure 5.14. The results show that the MSPRoA method generated good edge maps in the regions roads and fields. However, the method resulted a number of spurious edge pixels in the middle regions where several busy structures are closely placed. However, test results indicate that the MSPRoA method generated edge maps were better compared to the MRoA and RGoA edge maps.

The comparative study and analysis of MSPRoA edge maps on SAR images with the corresponding edge maps obtained using previous edge detection methods show that the MSPRoA method performed better on SAR images than the RGoA or MRoA methods. The boundaries between regions and fine details are well registered in the MSPRoA edge maps. The contours and lines are continuous and precise. Its performance on *Industrial* image was also found to be better compared to previous edge detection methods.



Figure 5.11: The MSPRoA results a comparative study on *Fields* :

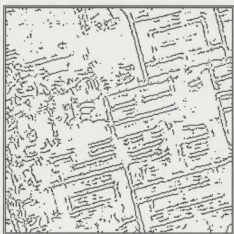
- (a) SAR test image *Fields* ;
- (b) The MRoA for (a) [$N = 7, T_r = 0.45$] followed by edge thinning;
- (c) The RGoA for (a) [$N = 9, T_r = 0.45, T_g = 50$] followed by edge thinning;
- (d) The MSPRoA for (a) [$N = 9, T_r = 0.6, d = 2$].



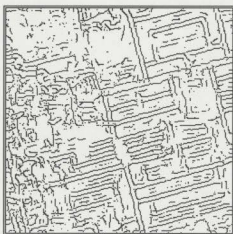
(a)



(b)



(c)



(d)

Figure 5.12: The MSPRoA results comparative study for SAR *Busy* :

- (a) SAR test image *Busy* ; (b) The MRoA [$N = 7, T_r = 0.475$] followed by edge thinning; (c) The RGoA on (a) [$N = 9, T_r = 0.475, T_g = 50$] followed by edge thinning; (d) The MSPRoA on (a) [$N = 9, T_r = 0.62, d = 2$].



(a)



(b)

Figure 5.13: The MSPRoA test results a comparative study on *Highway*
(a) SAR test image *Highway* ; (b) MRoA edge map on (a) [$N = 9, T_r = 0.45$] followed by edge thinning;



(c)

(d)

Figure 5.13: The MSPRoA results a comparative study on *Highway* : (c) RGoA edge map on (a) [$N = 9, T_r = 0.45, T_y = 50$] followed by edge thinning;
(d) The MSPRoA edge map on (a) [$N = 7, T_r = 0.6, d = 2$].

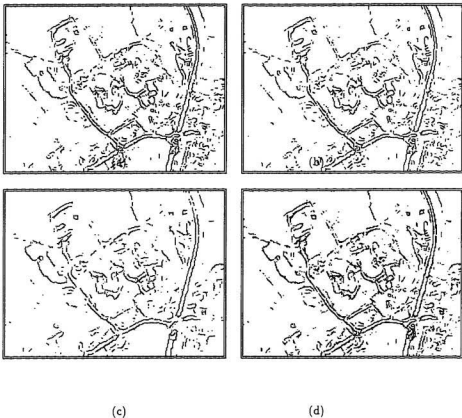


Figure 5.14: The MSRoA results a comparative study for SAR *Industrial* :
 (a) SAR image *Industrial* ; (b) MRoA edge map on (a) [$N = 9, T_r = 0.45$] followed by edge thinning; (c) RGoA edge map on (a) [$N = 9, T_r = 0.45, T_g = 50$] followed by edge thinning; (d) MSPRoA edge map on (a) [$N = 11, T_r = 0.63, d = 2$].

5.5 The MSPRoA edge tracking algorithm

The MSPRoA edge detection results studied further to determine conditions required to generate edge maps giving quality equal to the ideal edge maps. The MSPRoA test results on simple test image *Bars* are used for test and analysis.

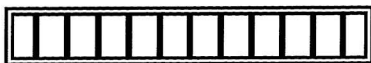
Figure 5.15(a) shows test image *Bars* used which is previously used in Chapter [4] of Figure 4.3. Figure 5.15(b) corresponding speckled image. The Sobel edge map on original *Bars* image is shown in Figure 5.15(c) and the MSPRoA edge map on speckled image shown in Figure 5.15(d).

Edge detection test results show that the MSPRoA method on synthetic images extracted edge maps with single pixel accuracy. Generated edge maps were thin and precise giving close approximation to ideal edge maps. Sobel operator on noise-free image generated edge map which is two pixels wide. However, the MSPRoA edge map shows some deviations compared with ideal edge map Figure 5.15(d). The method selected edge pixels from one of the two regions defining the edges.

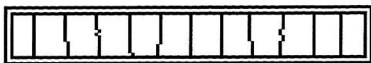
This effect was not accounted as error using Zaman and Moloney edge detectors quantitative performance measures since, these exists exact match in the corresponding ideal edge map. The MSPRoA method was also found to be successful according to Canny [7] as it satisfies single response to single edge conditions. Although, the effect was not accounted as an error, it has some effect on visual quality of generated edge maps. In this section a simple and fast MSPRoA edge tracking algorithm is suggested to improve visual quality of the MSPRoA generated edge maps.

The MSPRoA edge tracking algorithm:

If $P(i,j)$ is the MSPRoA detected edge pixel, then, the following sequence of steps are used to verify if relocation is required for $P(i,j)$ to improve visual quality of the



(a)



(b)

Figure 5.15: The MSPRoA edge tracking algorithm test results for *Bars*
(a) Sobel edge map for *Bars* ; (b) The MSPRoA edge map for speckled *Bars* :

MSPRoA edge maps using the MSPRoA edge tracking algorithm:

- For $K \leq tracklength$, number of edge pixels found in the lanes $l - 1$, l and $l + 1$ oriented in the direction $i + 90$ are measured where i is $P(i, j)$ edge orientation, l is lane (row/column) in which $P(i, j)$ is located and K user selected integer.
- The lane (row/column) that gives maximum number of edge pixels is considered as the lane L with highest probability rate for edge pixel $P(i, j)$ to be located.
- If $L = l$ edge pixel $P(i, j)$ need not relocate. else $P(i, j)$ is relocated to lane L .

The MSPRoA edge tracking algorithm test results on *Bars* image is shown in Figure 5.16(b). The MSPRoA edge tracking algorithm is also tested using *Strips*, *Ring* and *Combine* images to study its effect in improving visual quality of the edge maps.

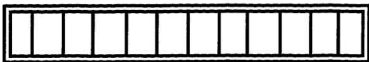
The MSPRoA edge tracking algorithm improves visual quality of the generated edge maps by suitably changing those edge pixels positions that are off the track compared with their neighboring edge pixels. The MSPRoA edge tracking algorithm found to most successful on test image *Strips* reproducing edge map with quality equal to the ideal edge map. Edge map is better compared to ideal edge map as edges separating regions are extracted with single pixel accuracy (Figure 5.17(c)). This test image used track length $k = 4$ for edge tracking purpose.

Test results on *Ring* image are obtained using track length $k = 2$. Test results on *Ring* test image are shown in Figure 5.17(d). Significant improvement in visual quality of generated edge map was not observed in case of *Ring* image as these image contained edge pixels that rapidly change their edge orientation.

Test results on *Combine* (Figure 5.18(b)) showed some improvement compared to its corresponding the MSPRoA edge map (Figure 5.18(a)). This image also used track length $k = 2$ value. Test image *Combine* shows some improvement may be due to



(a)



(b)

Figure 5.16: The MSPRoA edge tracking algorithm on *Bars*

- (a) Ideal edge map on noise-free *Bars* ;
- (b) The MSPRoA edge tracking algorithm;

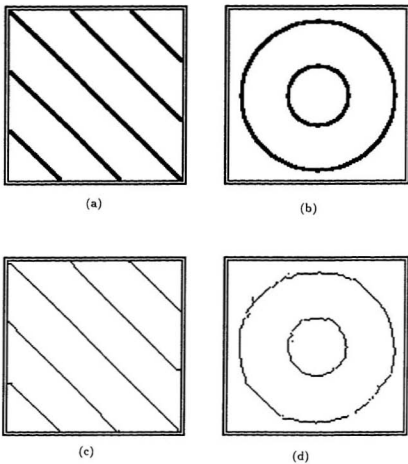
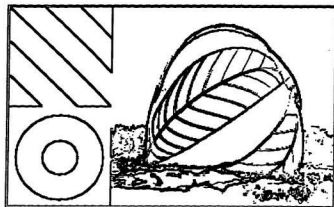
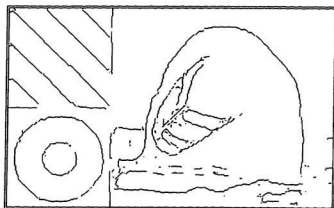


Figure 5.17: The MSPRoA edge tracking algorithm
 (a) *Strips* Ideal edge map; (b) *Ring* Ideal edge map;
 The MSPRoA edge tracking algorithm on (c) *Strips* ; (d) *Ring* :



(a)



(b)

Figure 5.18: The MSPRoA edge tracking algorithm on *Combine*
(a) Ideal *Combine* edge map; (b) Edge tracking on *Combine* MSPRoA.

the fact that image contained information that changes its edge orientation less often compared to *Ring* test image.

The MSPRoA edge tracking algorithm test results on synthetic test images show that the method is useful and improves visual quality of the generated edge maps. For effective use of this algorithm it is recommended to use small track length values in case image contains information on edge pixels that rapidly change their orientations compared with neighboring edge pixels.

The MSPRoA edge tracking algorithm is also tested using real airborne SAR images. Edge maps are obtained applying the MSPRoA edge tracking algorithm on *Fields*, *Highway* and *Industrial* using track lengths $k = 2$ for all the three images. Corresponding test images are shown in Figures 5.19(b), 5.20(b) and 5.21(b). The MSPRoA edge maps before applying edge tracking algorithm are shown in Figures 5.19(a), 5.20(a) and 5.21(a).

Test results show that the MSPRoA edge tracking algorithm improves visual quality of the edge maps generated using the MSPRoA method on real airborne SAR images. However, the effect was not significant as it was found on synthetic test image *Strips* (Figure 5.17(c)). Edge maps visual quality improvement on SAR images found similar to the test results observed on synthetic test image *Combine* (Figure 5.18(b)) which consisted variety of edge structures such as lines, wide arcs and sharp curves.

The MSPRoA edge tracking algorithm only provides a refined edge map on the MSPRoA generated edge maps. The algorithm is not useful for extracting additional information on images if edge map contains some true edge pixels information missing. Hence, information regarding the edge pixels that are missing still remain missing even after using the MSPRoA edge tracking algorithm. Multi-scale approach would be more suitable for extracting all true edges information simultaneously on both fine and large

image structures. A simple multi-scale MSPRoA method for extracting all true edges information on speckled images having variety of scene contents is suggested and is presented in the next section.

5.6 Multi-scale MSPRoA edge detector

5.6.1 Multi-scale MSPRoA on synthetic test images

The use of multi-scale approach in order to detect underlying image information has been used by several researchers in the past [82, 6]. The use of MSPRoA method for extracting edges at micro and macro levels is suggested in this section.

Figure 5.19(a) shows extracted sub-image of *Combine* (Figure 3.4(a)) showing fine details information on balloon in the *Combine* test image. The corresponding section of the image is extracted from speckled *Combine* (Figure 3.4(b)) and is shown in Figure 5.19(b). Test image shown in Figure 5.19(a) and (b) are used for test and analysis of working of the multi-scale MSPRoA method. The multi-scale MSPRoA method is then tested using synthetic and SAR test images. Test image shown in Figure 5.19(a) is referred using *Balloon* in this thesis.

Figure 5.19(c) shows ideal edge map on *Balloon* obtained using Sobel operator (equation 2.6). Figure 5.19(d) shows the MSPRoA edge map obtained on Figure 5.19(b) using $N = 5$, ratio-threshold value $T_r = 0.45$ $d = 2$. Figure 5.19(e) shows the corresponding MSPRoA edge map obtained using $N = 9$, ratio threshold value $T_r = 0.6$ and $d = 2$. Figure 5.19(f) shows combination of Figure 5.19(d) and (e) producing multi-scale MSPRoA edge map for the test image shown in Figure 5.19(b). Test results from Figures 5.19(c) and (f) show that the use of MSPRoA method at different mask sizes is successful in producing edge map on speckled *Balloon* producing edge map which also included find

details information.

The suggested multi-scale MSPRoA method uses different mask sizes and combines resulting edge maps using *OR* operator. The judgment on what mask sizes are to be selected and how many edge maps are to be used is to be made by the user keeping in view of the underlying image contents.

The multi-scale MSPRoA method is tested using *Combine* (Figure 3.4(a)) image. The corresponding test results are shown in Figure 5.20(b). Figure 5.20(a) shows Sobel edge map on original *Combine*. The multi-scale MSPRoA edge map combined using mask sizes $N = 5$, $N = 7$ and $N = 13$. Different ratio threshold values are used for different mask sizes in order to obtain clean edge maps reducing spurious edge pixel information in each case. Threshold values used are $T_r = 0.45$, $T_r = 0.55$ and $T_r = 0.63$ for $N = 5$, $N = 7$ and $N = 13$ mask sizes respectively. The correlation distance parameter value $d = 2$ is selected for all the mask sizes. The mask size $N = 5$ is selected for extracting fine details information. Mask size $N = 7$ is selected to support information extracted using $N = 5$ mask size. The selection of $N = 13$ is made to extract large structures information with clean boundaries.

The multi-scale MSPRoA edge map shown in Figure 5.20(b) shows additional information on edge pixels being extracted when compared to the MSPRoA edge map shown in Figure 5.3(d) which used mask size $N = 13$ only. Hence it may be possible to extract fine details and large details information simultaneously on speckled images using multi-scale MSPRoA method.

5.6.2 The Multi-scale MSPRoA on airborne SAR images

The multi-scale MSPRoA method is tested using the SAR test images *Fields*, *Highway*, and *Industrial*. Figure 5.21(a) shows the MSPRoA edge map on the *Fields*

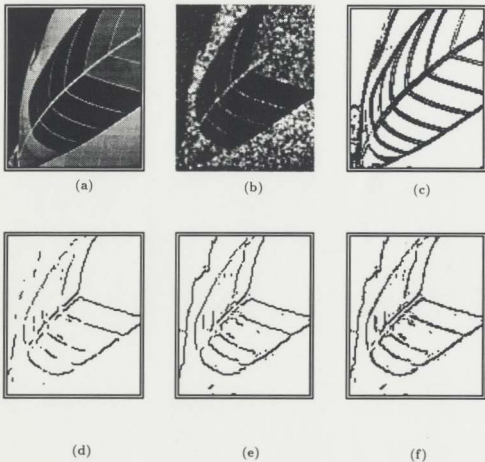
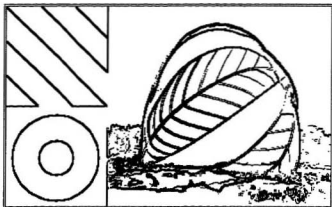
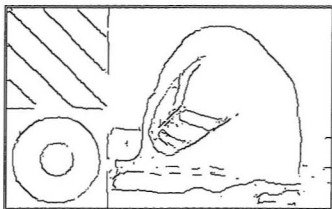


Figure 5.19: Multi-scale MSPRoA results for *Balloon*

(a) Original *Balloon* ; (b) Speckled *Balloon* ; (c) Sobel edge map for (a) [$T=100$];
 (d) MSPRoA edge map for (b) [$N = 5, T_r = 0.45, d = 2$]; (e) MSPRoA edge map
 for (b) [$N = 9, T_r = 0.6, d = 2$]; (f) Multi-scale MSPRoA combining (d) and (e).



(a)



(b)

Figure 5.20: Multi-scale MSPRoA result for *Combine* :

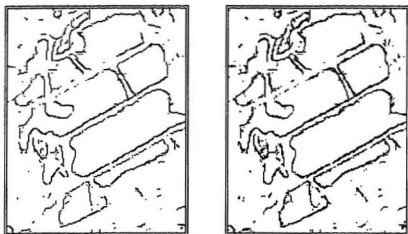
(a) Sobel edge map for 3.4(a) [$T=100$]; (b) Multi-scale MSPRoA for 3.4(b) using
 $[(N = 13, T_r = 0.63, d = 2) \text{ OR } (N = 7, T_r = 0.55, d = 2) \text{ OR } (N = 5, T_r = 0.45,$
 $d = 2)]$.

(Figure 5.4(a)) test image. Figure 5.21(b) shows the multi-scale MSPRoA edge map on the *Fields* obtained using $N = 5$, $T_r = 0.45$, $N = 9$, $T_r = 0.58$ and $N = 11$, $T_r = 0.62$. Correlation distance $d = 2$ is used for all mask sizes. The multi-scale MSPRoA edge map on the *Highway* test image is obtained considering test image shown in Figure 5.6(a). The multi-scale MSPRoA edge map is obtained using $N = 5$, $T_r = 0.45$ and $N = 7$, $T_r = 0.6$ is shown in Figure 5.22(b). The corresponding MSPRoA edge map obtained using $N = 7$, $T_r = 0.6$ and $d = 2$ is shown in Figure 5.22(a).

The multi-scale MSPRoA method is also tested using the SAR *Industrial* test image. Figure 5.23(a) shows the MSPRoA edge map on *Industrial* obtained using $N = 13$, $T_r = 0.62$ and $d = 2$. The MSPRoA edge map obtained using $N = 5$, $T_r = 0.45$ is shown in Figure 5.23(b). Figure 5.23(c) shows the corresponding MSPRoA edge map obtained using $N = 9$, $T_r = 0.58$, $d = 2$. Figure 5.23(d) shows multi-scale MSPRoA edge map which is a combination of the edge maps in Figure 5.23(a), (b) and (c) edge maps.

The test results using the multi-scale MSPRoA method on the SAR test images show that the method is successful in extracting edge pixel information, and in giving better definition on boundaries and details in these images. The method is found to be relatively better on the SAR test images *Fields* and *Industrial*. However, the test results on *Highway* did not show a significant improvement when compared with the corresponding test results using only one mask size.

Hence these results indicate that the multi-scale MSPRoA method may be used on images which consist of a variety of scene contents and business in order to extract edge maps with precision close to that of the human perceived edge maps.



(a)

(b)

Figure 5.21: The multi-scale MSPRoA on SAR test image - *Fields*

(a) The MSPRoA edge map for *Fields* [$N = 9, T_r = 0.6, d = 2$]; (b) The multi-scale MSPRoA edge map for *Fields* [$N = 7, T_r = 0.55, d = 2; N = 9, T_r = 0.6, d = 2$];



(a)

(b)

Figure 5.22: The multi-scale MSPRoA test results on SAR *Highway*

(a) MSPRoA edge map for *Highway* [$N = 7$, $T = 0.6$, $d = 2$]; (b) Multi-scale MSPRoA edge map for *Highway* [$N = 5$, $T = 0.45$, $d = 2$; $N = 7$, $T = 0.6$, $d = 2$];

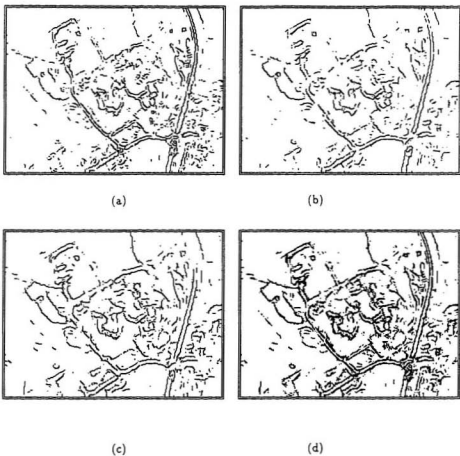


Figure 5.23: The multi-scale MSPRoA test results on SAR *Industrial* :

- (a) MSPRoA edge map using $[N = 5, T_r = 0.35, d = 2]$; (b) MSPRoA edge map using $[N = 7, T_r = 0.55, d = 2]$; (c) MSPRoA edge map using $[N = 11, T_r = 0.63, d = 2]$; (a) Multi-scale MSPRoA edge map for *Industrial* using (a), (b) and (c).

Chapter 6

Conclusions and Future Studies

6.1 Conclusions

Edge detection in the case of speckled images is important as these images are found in a variety of digital image processing application fields using laser, sonar, radar, SAR, ultrasound images etc., Speckle noise differs from other types of noise such as additive white Gaussian noise (AWGN) commonly observed in digital images in that it is multiplicatively signal dependent and may be spacially highly correlated. Speckle makes it difficult to extract true edges information due to its multiplicative signal dependent nature.

Ordinary gradient edge detection methods which use differences between pixel values tend to give inconsistent estimates when they were applied to speckled images. For this reason, such edge detection methods perform poorly on speckled images [3, 23, 90]. Ratio based method which use ratios of pixels values as a measure of edge strength tend to cancel out the multiplicative noise effect present in speckled images. When applied to speckled images these methods are successful in giving better estimates regarding true edge pixels on speckled images.

However, previous ratio based methods generate thick edge maps. Evaluations of existing speckle specific edge detection methods show that these methods do not extract all and only true edge pixels information on speckled images. An attempt to extract all true edge pixels information using existing ratio based methods may give thick edge maps and may also include some wrong edge pixels. On the other hand, attempts to reduce the number of wrong edge pixels result in an increase in the number of missing edge pixels. Although these previous ratio based methods can give satisfactory results on speckled image, they may not be successful in generating edge maps that give close estimates to corresponding ideal edge maps.

SAR images with actual speckle noise have been used with permission from Canada Center for Remote Sensing (CCRS) to study and analyze existing edge detection methods for speckled images. Previous evaluations on edge detection methods for speckled images used synthetic test images. The evaluation of edge detection methods for real airborne SAR images presented in this thesis also confirm suitability of ratio methods for use on speckled images. Zaman and Moloney [90] MRoA and RGoA edge detection methods on real SAR images were found to perform relatively better compared with the other speckle specific edge detection methods. However, these methods also generate thick edge maps and require edge thinning operations. The edge maps also consists of missing edge pixel information compared to the human perceived edge maps for these images.

The previous ratio based edge detectors studied in this thesis utilized only edge magnitude information in extracting true edge pixels information. However since the most recent methods also determine edge orientation information, it is suggested that edge orientation information may also be useful in extracting true edge information and in providing better estimates regarding ideal edge pixel information.

The Maximum Strength edge Pruned Ratio of Averages (MSPRoA) method attempts

to extract true edge information from speckled images by making effective use of edge orientation information. The MSPRoA successfully extracts true edge pixel information by pruning edge pixels based on both magnitude and direction edge strength values. The MSPRoA method is successful in generating thin, localized and well defined edge maps for synthetic speckled images. The edge detector quantitative performance measures for these detected edge maps are close to the measures obtained for ideal edge maps. The generated edge maps do not require edge thinning post-processing or gradient edge strength calculations and hence computational savings are achieved.

The MSPRoA method was found to be successful in extracting true edge pixel information when applied to airborne SAR images of varying scene contents and business. The method was found to be successful in extracting information for SAR images having both fine and large structures (as seen from the results on the *Fields*, *Busy* and *Highway* SAR images). Very fine detail information was also successfully extracted using the MSPRoA method as can be seen from the edge maps for the *Highway* SAR image which yields information on cars moving on the highway lanes.

The MSPRoA method extracts edge pixels from speckled images with single pixel accuracy. At times, the method extracts edge pixels from the two regions to either side of the edge. In such applications, a fast edge tracking algorithm is suggested for use with MSPRoA edge maps in order to improve the visual quality of the generated edge maps. The MSPRoA edge tracking algorithm improves visual quality of the edge maps for images with edge pixels that do not rapidly change their edge orientation compared with their neighboring edge pixel edge orientations (as in the synthetic *Strips* image). The edge tracking algorithm should be used with a small track length value K on images containing image structures with rapidly changing edge orientations such as arcs or sharp contours (ex. *Combine*, *Ring*). The MSPRoA edge tracking test results on SAR

images improvement in the visual quality of the generated edge maps by better defining the boundaries between regions. Hence, the MSPRoA method may be used in image registration, classification or object recognition in SAR images. Charles Robertson and Moloney used MSPRoA for automated registration of SAR images [79].

The MSPRoA edge detection method was found to perform relatively poor on images having very fine details and large structures. Since, the MSPRoA edge tracking algorithm only rearranges edge pixels found using the MSPRoA method, this method can not extract true edge pixels not detected by MSPRoA method. The MSPRoA method and MSPRoA edge tracking algorithm performed poorly on images having variety of image structures simultaneously (ex. *Combine* and *SAR Industrial*). In such cases the use of MSPRoA method at multiple scales could successfully extract a number of true edge pixels information at micro and macro scales simultaneously.

The MSPRoA method at multiple scales-performed better than the simple MSPRoA method when applied to images containing a variety of image information. The multi-scale version of the MSPRoA method uses different mask sizes suitable to extract edge information for both fine and large image structures. Based on test results the multi-scale MSPRoA method is recommended on images containing variety of image structures.

6.2 Future Studies

Overall, the MSPRoA method was found to be successful in detecting edges on speckled images containing fine, moderate and large structures. The edge detection results obtained using the MSPRoA method on real airborne SAR images show that the method determines precise edge maps. However, the method performed relatively

poorly on images containing variety of structures.

The multi-scale MSPRoA method performed well on the synthetic test image *Combine* and SAR test image *Highway*. Although the MSPRoA method at multi-scales using different mask sizes performed well, some true edge pixel information continues to be missing and can be seen from the test results for SAR *Industrial* test image. The MSPRoA method may be improved in order to extract all and only true edge pixel information on images having a variety of image structures.

The MSPRoA edge detector performance may be improved further using multi resolution image pyramids or sub-band decomposition of the input image [6]. Use of image pyramids followed by contour following edge linking algorithms to join edge pixels detected at different resolution scales may also improve existing MSPRoA algorithm performance.

References

- [1] M. Adair and B. Guindon, "Methods for evaluating speckle suppressing filters based on edge detection performance," *Canadian Journal of Remote Sensing*, Vol. 15, No. 2, pp. 101-108, Sept. 1989.
- [2] A. C. Bovik and D.C. Munson, "Boundary detection in speckle images," *Proc. Intl. Conf. Acoust., Speech, Signal Processing, ICASSP'85* (Tampa, FL), Mar. 1985. pp. 24.2.1-24.2.4.
- [3] A.C. Bovik, "On detecting edges in speckle imagery," *IEEE Trans. on Acoustics Speech and Signal Processing*, Vol. 36, pp. 1618-1627, 1988.
- [4] B.J. Thompson, "Image formation with coherent light - A tutorial review." *Coherent Opt. Engineering*, New York: North Holland, Oxford, pp. 49-61. 1976.
- [5] B. Brisco, R.J. Brown, and M.J. Manore. "Early season crop discrimination with combined SAR and TM data," *Canadian J. Remote Sensing*, Vol. 15, No. 1, pp. 44-54, 1989.
- [6] J. Peter. Burt, and E. H. Adelson, "The Laplacian Pyramid as a Compact Image Code." *IEEE Trans. on Communications*, Vol. COM-31, No. 4, pp. 532-540, 1983.

- [7] J. Canny, "Finding edges and lines in images," Technical Report 720. Artificial Intelligence Labs M.I.T., June 1983.
- [8] J. Canny, "A computational Approach to Edge Detection," *IEEE Trans. Pattern Anal. Machine Intell.*, Vol. PAMI-8, No. 6, pp. 679-698, Nov. 1986.
- [9] J.S Chen and G. Medioni, "Detection, Localization and Estimation of Edges," *IEEE Trans. Pattern Anal. Machine Intell.*, Vol. PAMI-11, pp. 191-198, 1989.
- [10] J.C. Dainty, "The statistics of speckle patterns," *Progress in Optics*. Vol. XIV, pp. 3-46. E. Wolf, Ed., The Netherlands:North-Holland, 1976.
- [11] L.S. Davis, "A survey of Edge detection Techniques," *Computer Graphics and Image Processing*, Vol. 4, No. 3, pp. 248-270, 1975.
- [12] L. Davis and A. Rosenfeld, "Detection of step edges in noisy Images," *IEEE Trans. on Computers*, pp. 1006-1010, 1975.
- [13] L. Davis, "A survey of edge detection techniques," *Computer Graphics and Image Procc.*, Vol. 16, pp. 158-165, 1981.
- [14] L. Davis and A. Mitchie "Edge detection in Textures - Maxima Selection," *Computer Graphics and Image Processing*, Vol. 16, pp. 158-165, 1981.
- [15] H. Derin, P.A. Kelly, G. Vezina, and S.G. Labitt, "Modeling and segmentation of speckled images using complex Data," *IEEE Trans. on Geosci. and Remote Sensing*, Vol. GE-28, No. 1, Jan. 1990.
- [16] R.O. Duda and P.E. Hart, *Pattern recognition and scene analysis*, New York: Wiley, 1973.

- [17] J.M. Durand, B.J. Gimonet, and P.R. Perbos. "SAR Data filtering for classification." *IEEE Trans. Geosci. and Remote Sensing*, Vol. GE-25, No. 5, pp. 629-637, Sept. 1987.
- [18] R. Eberlein. "An Iterative Gradient Edge detection Algorithm." *Computer Graphics and Image. Proc.* Vol. 5, pp. 245-253, 1976.
- [19] R. Ehrlich. "Detection of Global Edges in Textured Images." *IEEE Trans. on Computers*, Vol. C-26, pp. 589-603, 1977.
- [20] J.O. Eklundh, T. Elfing, and S. Nyberg, "Edge detection using Marr-Hildreth Operator with different sizes," *Proceedings of Sixth Intl. Conf. on Pattern Recognition 1982*, Munich pp. 1109-12.
- [21] M.R.B. Forshaw, "Speeding up the Marr-Hildreth Edge Operator." *Computer Vision, Graphics, and Image Processing*, Vol. 41, pp. 172-185, 1988.
- [22] J.R. Fram and E.S. Dentsch. "On the quantitative evaluation of edge detection schemes and their comparison with human performance." *IEEE Trans. on Computers*, Vol. C-24, pp. 616-628, 1975.
- [23] V.S. Frost, J.A. Stiles, K.S. Shanmugan, and J.C. Holtzman, "A model for radar images and its application to adaptive digital filtering of multiplicative noise." *IEEE Trans. Pattern Anal. Machine Intell.*, Vol. PAMI-4, pp 157-166, Mar. 1982.
- [24] V.S. Frost, K.S. Shanmugan, and J.C Holtzman, "Edge detection for synthetic aperture radar and other noisy images." Remote Sensing Laboratory, University of Kansas Center for Research, Inc., Lawrence, Kansas, USA.

- [25] D. Denby, G.E. Quintanilla, and J.N. Butters, *The engineering uses of Coherent Optics*, Cambridge University Press: London, 1976.
- [26] D.A. Gregory, *The Engineering Uses of Coherent Optics*. Cambridge University Press, 1976.
- [27] R.K. Erf, *Speckle Metrology*, New York: Academic, 1978.
- [28] S.J. Arnold, W.L. Boksenberg, and L.M. Sargent, *Astrophys J.*, 1986.
- [29] J.W. Harvey, *Astrophys J.*, 1973
- [30] H.A. McAlister, *Astrophys J.* 215 159, 1977
- [31] A.K. Gabriel, R.M. Goldstein, "Crossed orbit interferometry: Theory and experimental results from SIR-B," *J. Remote Sensing*, Vol. 9, No. 8, pp. 857-872, 1988.
- [32] S.S. Ganugapati and C. R. Moloney, "Maximum Strength Edge Pruned Ratio of Averages Edge Detector for Speckled Images," *Proc. Newfoundland Electrical and Computer Engineering Conference, NECEC-1995*, St. John's, Canada, May, 1995.
- [33] S.S. Ganugapati and C. R. Moloney, "A Ratio edge detector for speckled images based on maximum strength edge pruning," *IEEE International Conference on Image Processing (ICIP-95)*, Washington, D.C., USA, Oct. 23-26, 1995.
- [34] J.W. Goodman, "Statistical properties of laser speckle patterns," in *Laser Speckle and Related Phenomena*, J.C Dainty, pp. 9-75, Ed. Heidelberg: Springer-Verlag, 1975.
- [35] A.L. Gray and Farris-Manning, "Repeat-pass interferometry with airborne synthetic aperture radar," *IEEE Trans. Geosci. Remote Sensing*, Vol. 31, No.1, pp. 180-191, 1993.

- [36] E. V. Guy, and R.H. Khan. "Three-channel Wiener Filter for Suppression of Speckle noise in SAR images of Ocean Scenes." *Proc. NECEC-95*, St. John's, Canada.
- [37] R.O. Harger, *Synthetic Aperture Radar Systems*, New York:Academic. 1970.
- [38] R.M. Haralick, "Edge and Region Analysis for Digital Image Data." *Computer Vision, Graphics, and Image Processing*, Vol. 12, pp. 60-73, 1980.
- [39] R.M. Haralick, "Digital step edges from zero crossings of second directional derivatives." *IEEE Trans. on Pattern Anal. and Machine Intell.*, PAMI-1. pp. 58-68. 1984.
- [40] R.M. Haralick and G.S. Linda, "Computer and Robot Vision." Addison-Wesley Publishing Co.. 1992.
- [41] R. Hartley, "A Gaussian-Weighted Multiresolution Edge Detector," *Computer Vision. Graphics, and Image Processing*, Vol. 30, pp. 70-83, 1985.
- [42] K.D. Hartt, P.A. Kelly and H. Derin, "The modeling and segmentation of speckled images," *Proc. 1987 Intl.Conf. Acoust. Speech, Signal Processing ICASSP-87* (Dallas, Texas), Apr. 1987, pp. 14.3-14.3.4.
- [43] T.K. Hirose, T.J. Pultz and E.J. Langham, "An Evaluation of Noise Reduction Algorithms for Data Corrupted by Multiplicative Noise," *Canadian J. Remote Sensing*, Vol. 15, No. 1, May. 1989.
- [44] T. Hong, *et.al.* "Image Smoothing and Segmentation by Multiresolution Pixel Linking: Further Experiments and Extensions," *IEEE Trans. on Sys., Man, Cybern.* Vol. SMC-12, pp. 611-622. 1982.

- [45] T. Hong, M. Shneier and A. Rosenfeld, "Border extraction using linked Edge Pyramids." *IEEE Trans. on Syst., Man, Cybern.*, Vol. SMC-12, pp. 660-668, 1982.
- [46] J.S. Huang and D.H. Tseng, "Statistical Theory of Edge Detection." *Computer Vision, Graphics, and Image Processing*, Vol. 43, pp. 337-346, 1988.
- [47] D.V. Hudson and M.E. Jernigan, "Speckle suppressing and texture in synthetic aperture radar images," *Technical report # 160-I-120988*, Tech. Report. Department of Systems Design Engineering, University of Waterloo, Canada.
- [48] T. Kasvand, "Iterative Edge Detection." *Computer Vision, Graphics, and Image Processing*, Vol. 4, pp. 279-286, 1975.
- [49] P.P. Kelly, H. Derin and K. Hartt, "Adaptive Segmentation of Speckled Images Using a Hierarchical Random Field Model." *IEEE Trans. on acoustics, Speech and Signal Proc.*, Vol. 36, No. 10, pp. 1628-1641, 1988.
- [50] L. Kitchen and A. Rosenfeld, "Edge evaluation using local edge coherence." *IEEE Trans. on Syst., Man, Cybern.*, Vol. SMC-11, pp. 597-605, 1981.
- [51] D.T. Kuan, A.A. Sawchuk, T.C. Strand and P. Chavel, "Adaptive Noise Smoothign Filter for Images with Signal-Dependent Noise," *IEEE Trans. on Patten. Anal. Machine Intell.*, Vol. PAMI-7, No.2, pp. 165-177, 1985.
- [52] D.T. Kuan, A.A. Sawchuk, T.C. Strand and P. Chavel, "Adaptive restoration of images with speckle," *IEEE Trans. Acoust. Speech, Signal Processing*, Vol. ASSP-35, pp 373-383, 1987.

- [53] J.S. Lee. "Digital image enhancement and noise smoothing by use of local statistics." *IEEE Trans. Pattern Anal. and Machine Intell.*, Vol. PAMI-2, No. 2, pp. 165-171, 1980.
- [54] J.S. Lee, "Speckle analysis and smoothing of synthetic aperture radar images." *Comput. Graph. Image Processing*, Vol. 17, pp. 24-32, 1981.
- [55] J.S. Lee. "A Simple speckle smoothing algorithm for Synthetic Aperture Radar images." *IEEE Trans. Syst., Man, Cybern.*, Vol. SMC-13, pp 85-89, 1983.
- [56] J.S. Lee, "Digital image smoothing and sigma filter." *Comput. Vision, Graphics and Image Process.*, Vol. 24, pp. 255-269, 1983.
- [57] J.S. Lee. "Speckle suppression and analysis of synthetic aperture radar images." *Opt. Eng.*, Vol. 25, No. 9, pp. 636-643, 1986.
- [58] J.S. Lee and I. Jurkevich, "Segmentation of SAR Images," *IEEE Trans. Geosci. and Remote Sensing*, Vol. 27, No. 6, pp. 674-678, 1989.
- [59] J.S. Lee, R. Grunes and S.A. Mango, "Speckle Reduction in Multipolarization Multifrequency SAR Imagery," *IEEE Trans. Geosci. and Remote Sensing*, Vol. 29, No. 4, pp. 535-543, 1991.
- [60] F. Li, C. Croft and D.N. Held, "Comparison of several techniques to obtain multi-look SAR imagery," *IEEE Trans. Geosci. Remote Sensing*, Vol. 21, No. 3, pp. 370-375, 1981.
- [61] A. Lopes, R. Touzi and E. Nezry, "Adaptive Speckle Filters and Scene Heterogeneity," *IEEE Trans. on Geosci. and Remote Sensing*, Vol. 28, No. 6, pp. 992-1000, 1990.

- [62] R. Machuca and A.L. Gilbert, "Finding Edges in Noisy Scenes," *IEEE Trans. Pattern Anal. and Machine Intell.*, Vol. PAMI-3, pp. 103-111, 1981.
- [63] D. Marr and E.C. Hildreth, "The theory of edge detection," *Proc. Roy. Soc. London B*, Vol. 207, pp. 187-217, 1980.
- [64] D. Marr, "Representing visual information." *Computer vision systems*. pp. 61-80. New York:Academic Press.
- [65] D. Marr, "Early processing of visual information," *Phil. Trans. R. Soc. Lon. B*. Vol. 275, pp. 483-524, 1976.
- [66] G.F. McLean and M.E. Jernigan, "Hierarchical Edge Detection." *Compt. Vision. Graphics, and Image Processing*, Vol. 44, pp. 350-366, 1988.
- [67] T.S. McKechnie, *Optics 39, 258*, 1974.
- [68] J.W. Modestino and R.W. Fries, "Edge detection in Noisy Images using Recursive Digital Filters," *Computer Graphics and Image Processing*, Vol. 6. pp. 409-433, 1977.
- [69] C.R. Moloney and G.S. Ganugapati, "Evaluation of edge detection methods for Airborne Synthetic Aperture Radar Images." *Proc. Newfoundland Electrical and Computer Engineering Conference, NECEC-1994*, St. John's, Canada. April. 1993.
- [70] M. Nagata, "Image Processing for Boundary Extraction of Remotely Sensed Data." *Pattern Recognition*, Vol. 4, pp. 275-282, 1981.
- [71] V.S. Nalwa and T.O. Binford, "On Detecting Edges," *IEEE Trans. Pattern Anal. Machine Intell.*, Vol. PAMI-8, pp. 699-714, 1986.

- [72] D.P. Panda and T. Dubitzki, "Statistical Analysis of Some Edge Operators," *Computer Graphics and Image Processing*, Vol. 11, pp. 313-348, 1979.
- [73] T. Peli and D. Malah, "A Study of Edge detection Algorithms," *Computer Graphics and Image Processing*, Vol. 20, pp. 1-21, 1982.
- [74] I. Pitas and A.N. Venetsanopoulos, "Edge detectors Based on Non-linear Filters," *IEEE Trans. Pattern Anal. and Machine Intell.*, Vol. PAMI-2, pp. 16-27, 1980.
- [75] T. Poggio, "Regularized solution to edge detection," Memo 833, *Artificial Intelligence Labs. AI, M.I.T.*, 1985.
- [76] L.J. Porcello, N.G. Massey, R.B. Innes and J.M. Marks, "Speckle reduction in synthetic aperture radars," *J.Opt. Soc.Amer.*, Vol. 66, pp. 1305-1311, 1976.
- [77] W.K. Pratt, *Digital Image Processing*, New York: Wiley-Interscience, 1978.
- [78] T.J. Pultz, R.J. Brown, "SAR image classification of agricultural targets using first and second order statistics," *Canadian Journal Remote Sensing*, Vol. 13, No. 2, pp. 85-91, 1987.
- [79] A.C. Robertson and C.R. Moloney, "Automated Registration of SAR Images," *Proc. Newfoundland Electrical and Computer Engineering Conference NECEC-1996*, St. John's, Canada, 1996.
- [80] A. Rosenfeld, *Picture processing by Computer*, New York: Academic, 1968.
- [81] A. Torre and T. Poggio, "On edge detection," *IEEE Trans. Pattern Anal. Machine Intell.*, Vol. PAMI-8, pp. 147-163, 1986.

- [82] R. Touzi, A. Lopes and P. Bousquet, "A statistical and geometrical edge detector for SAR images," *IEEE Trans. on Geosci. and Remote Sensing*, Vol. 26, pp 764-773, 1988.
- [83] P.M. Treitz and J.P. Howarth, "Classification of agricultural crops using SAR tone and textures," *Proc. 16th Canadian Symp. Remote Sensing*, Sherbrooke, Quebec, Canada, June 7-10, pp. 343-347, 1993.
- [84] E.E. Triendl, "How to get Edge into the Map," *Proceedings of Fourth Intl. Joint Conf. on Pattern Recognition*, pp. 946-950, Tokyo, 1978.
- [85] M. Tur, K.C. Chin and J.M. Goodman, J.W, "When is speckle noise multiplicative?," *Appl. Opt.*, Vol. 21, pp. 1157-1159, 1982.
- [86] F.T. Ulaby, F. Kouyate, B. Brisco, Lee, and T.H. Williams, "Textural Information in SAR Images," *IEEE Trans. on Geoscience and Remote Sensing*, Vol. GE-24, No. 2, pp. 235-245, 1986.
- [87] V.L.J. Vliet, I.T. Young and G.L. Beckers, "A Non-Linear Laplace Operator as Edge Detector in Noisy Images," *Computer Vision, Graphics, and Image Processing*, Vol. 45, pp. 167-195, 1989.
- [88] S. Ward, "Digital signal and image processing of airborne sidelooking SAR." *NSERC USRA Report*, Memorial University of Newfoundland, Sept. 1993.
- [89] M.R. Zaman, "Adaptive Filters for Edge-preserving Smoothing of Speckle Noise in Digital Images," *M.Eng. thesis*, Memorial University of Newfoundland, 1993.
- [90] M.R. Zaman and C.R. Moloney, "A comparison of adaptive filters for edge-preserving smoothing of speckle noise," *Proceedings of the 1993 International Con-*

ference on Acoustics, Speech and Signal Processing (ICASSP93), pp. V77-80. Minneapolis, Minnesota, 1993.

- [91] M.R. Zaman and C.R. Moloney, "Evaluation of edge detection methods for images with non-additive noise," *Processings of NECEC 93*, St. John's, Nfld, 1993.
- [92] H.A. Zebker and R.M. Goldstein, "Topographic mapping from inteferometric SAR observations." *J. Geophys. Res.*, Vol. 91, No. B5, pp. 4993-4999, 1986.
- [93] H.A. Zebker, C.L. Werber, P.A. Rosen and Hensley, "Accuracy of topographic maps derived from ERS-1 interferometric radar," *IEEE Trans. Geosci. Remote Sensing*, Vol. 32, No. 4, pp. 823-836, 1994.



